E2F Regulation Controls the Temporal Specificity of *Ccna2* Expression During Spermatogenesis

Research Thesis

Presented in partial fulfillment of the requirements for graduation with research distinction in Molecular Genetics in the undergraduate colleges of The Ohio State University

by

Manuel Torres

The Ohio State University - August 2017

Project Advisor: Gustavo Leone, Department of Cancer Biology

Abstract

The cell cycle, which comprises the series of events that lead to a cell's division, is regulated by a family of proteins called the Cyclins. These have fluctuating levels of expression across different stages of the cell cycle, and are regulated by the E2F family of transcription factors; these can bind to a specific consensus sequence and can activate and repress gene expression. One of their targets is Cyclin A2 (*Ccna2*/CCNA2), a cyclin that plays a major role in DNA synthesis and entry into the mitotic or meiotic phase. The *in vivo* relevance of E2F regulation, particularly of specific targets like *Ccna2* is not yet fully understood, and its study is important to understanding the conserved nature of the protein throughout evolution. To evaluate the importance of E2F-mediated regulation of *Ccna2 in vivo*, we generated a mouse line with a knock-in mutation at the putative E2F binding site of the *Ccna2* promoter. Although mice are viable and appear healthy, we observed infertility and early testicular atrophy in males homozygous for the promoter mutation. Using histological analysis, real-time PCR (qPCR), and antibody-mediated visualization of CCNA2 and stem cell marker localization in testes, we identified a defect in spermatogenesis initiation and sustenance, an aberrant *Ccna2* expression profile, and a late but sustained upregulation of stem cell activity throughout development. Collectively, these data suggest that the precise E2F-mediated regulation of *Ccna2* transcription is required for proper stem cell differentiation during spermatogenesis. The genomic acquisition of E2F binding sites can, therefore, be said to serve as an evolutionary mechanism that can bestow conserved proteins novel functions in different tissues. Further inquiry into how these transcription factors regulate their individual targets and how this regulation is important *in vivo* is likely to continue revealing novel functions and phenotypes, increasing our understanding of the cell cycle and the many ways it is and could be involved in human disease.

I. **Background**

A. The Cell Cycle

The cell cycle comprises the series of events that lead to a cell's division. In the G_1 phase, the cell prepares for DNA synthesis and commits to cell division. During the S and G2 phases, the DNA is replicated and the cell continues to grow and prepare for division, respectively (Rédei, 2008). Finally, the cell divides at the M phase into two identical daughter cells (mitosis) or into four haploid germ cells (meiosis).

This process is regulated by a family of proteins called the *Cyclins*, which have fluctuating levels of expression across different stages of the cell cycle (Figure 1A) (Morgan, 2007). These bind to and activate *Cyclin-dependent kinases* (*Cdks*), which in turn transfer phosphate groups to their targets and drive the cell cycle (Figure 1B) (Satyanarayana & Kaldis, 2009). *Cyclins*, like many other cell cycle proteins, are regulated by the E2F family of transcription factors. E2Fs bind to a specific consensus sequence and either activate (E2F1-E2F3) or repress (E2F4-E2F8) gene expression (Thurlings & Bruin, 2016). One of their targets is Cyclin A2 (*Ccna2*/CCNA2), a cyclin that plays a major role in DNA synthesis and entry into the M phase.

CCNA2 is necessary for life; *Ccna2*$^{-/-}$ mice are nonviable and die shortly after the implantation stage, when maternal *Ccna2* transcripts are depleted and the zygote is unable to induce cell proliferation (Wolgemuth *et al.*, 2008). It has also been shown to be upregulated in multiple cancers (Gao *et al.*, 2014) and has been suggested to promote tumorigenesis when overexpressed due to its potent induction of chromosomal Double-Strand Breaks (DSBs) (Shoji & Taku, 2009). During the cell cycle, it forms two complexes with *Cdks*. The CCNA2/CDK2 complex phosphorylates targets in the S-phase and drives processes involved in DSB induction and repair for meiotic recombination, Synaptonemal Complex formation (Ortega *et al.*, 2003), and telomere tethering (Viera *et al.*, 2014). CCNA2/CDK1 on the other hand functions at the G2/M transition by phosphorylating proteins that prevent DNA re-replication, DNA segregation, as well as cell morphogenesis during meiosis (Enserink, & Kolodner, 2010).

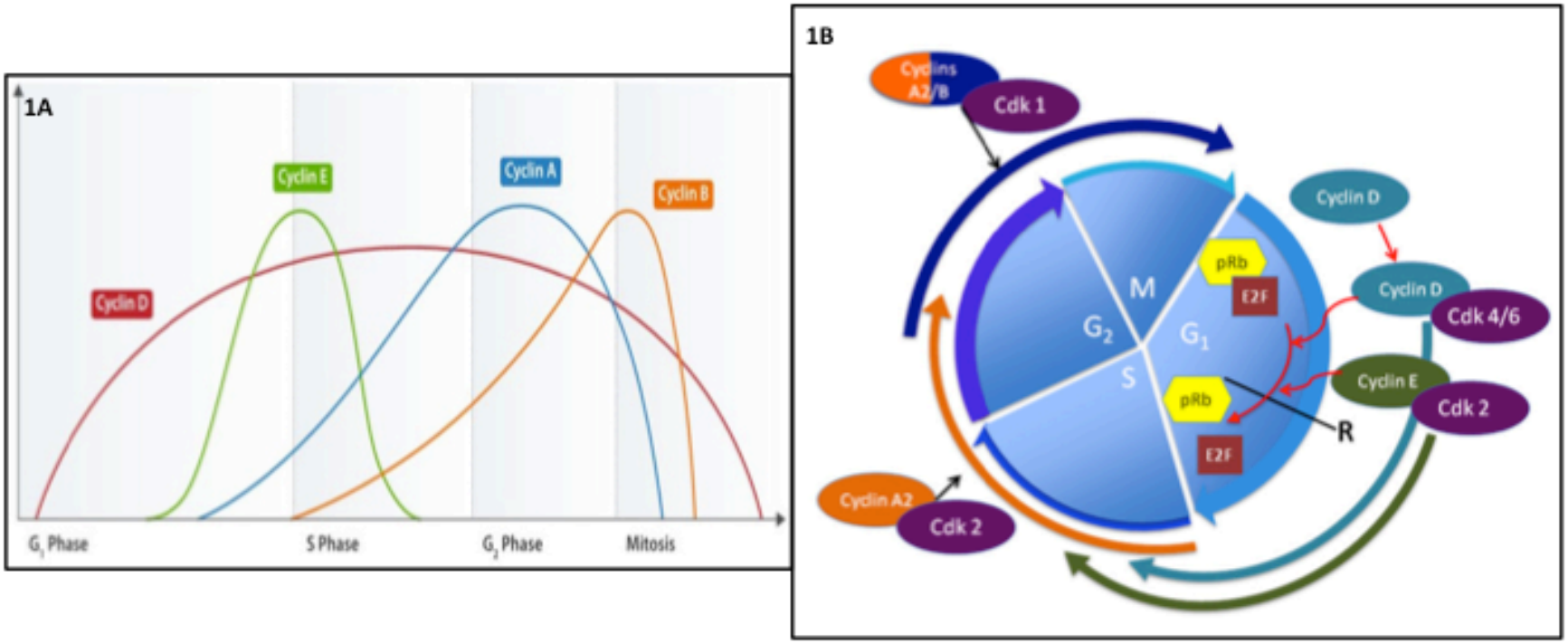

Figure 1: Regulation of the Cell Cycle. (A) Relative expression of *Cyclins* by cell cycle stage. (Image obtained from Revolvy.com) (B) Regulation of the cell cycle by Cyclins, Cdks and E2Fs. The CCNA2/CDK2 complex phosphorylates targets during the S-phase and part of the G2 phase, while CCNA2/CDK1 targets phosphorylates its targets during the G2/M phase transition, as seen in the figure. Figure modified from Wolgemuth *et al* (2008).

B. Meiosis: Spermatogenesis

Spermatogenesis is the process through which gametes are produced from pluripotent cells called spermatogonial stem cells (SCCs, PLZF-positive) that divide into differentiating spermatogonia (diff-SSC), which in turn differentiate into subsequent progenitor cells (spermatocytes) until haploid cells (spermatozoa) are produced (Hermo, 2014) (Figure 2A). This pool of SCCs is mainly located around the base of the seminiferous tubules in the testis and is maintained by a set of sustentacular cells called Sertoli cells and Leydig cells, which secrete hormones that drive spermatogenesis (Rebourcet *et al.*, 2014). The differentiating progenitor cells migrate towards the center of the tubule (lumen) where they accumulate as spermatogenesis progresses; this process is induced intermittently in different parts of the adult testis.

Due to their distinct expression profiles throughout the mitotic cell cycle, *Cyclins* also have a characteristic niche of expression across spermatogenic populations. In the case of *Ccna2* expression, it is expressed in mitotic stem cells (SSCs and diff-SSC) as well as in early meiotic preleptotene spermatocytes (Figure 2B) (Wolgemuth *et al.*, 2013). It's homologue, *Cyclin A1 (Ccna1)* has a specialized role in meiosis and is expressed from the mid-pachytene stage to the metaphase of the 1st meiotic division. *Ccna1*$^{-/-}$, along with *Cdk2*$^{-/-}$ male mice arrest at the pachytene stage due to the spermatocytes' inability to resolve the DSBs induced as part of meiotic recombination (Szostak *et al.*, 1983; Ortega *et al.*, 2003); these DSBs are marked by the histone variant phospho-yH2AX (p-yH2AX) (Mahadevaiah *et al.*, 2001). On the other hand, *Cdk1*$^{-/-}$ embryos, like those lacking *Ccna2*, are not viable (Diril *et al.*, 2012). Therefore *Ccna2* and *Cdk1* appear to hold the conserved roles in the cell cycle while *Ccna1* and *Cdk2* have specialized, non-redundant functions.

The expansion of SSCs after gonocyte differentiation during the 1st wave of spermatogenesis is crucial for fertility (Figure 3) (Lipshultz *et al.*, 2009). At postnatal day 3, the gonocyte population (SSC precursors) differentiates completely into two Spermatogonial populations: SSCs and diff-SSCs (Manku & Culty, 2015). This differentiating subpopulation is responsible for the 1st wave of sperm production (Figure 4), while the latter supplies the subsequent waves (Yoshida *et al,* 2004). During the following weeks, seminiferous tubules continue progressing through spermatogenesis synchronously until the 1st wave culminates around the 6th week of age.

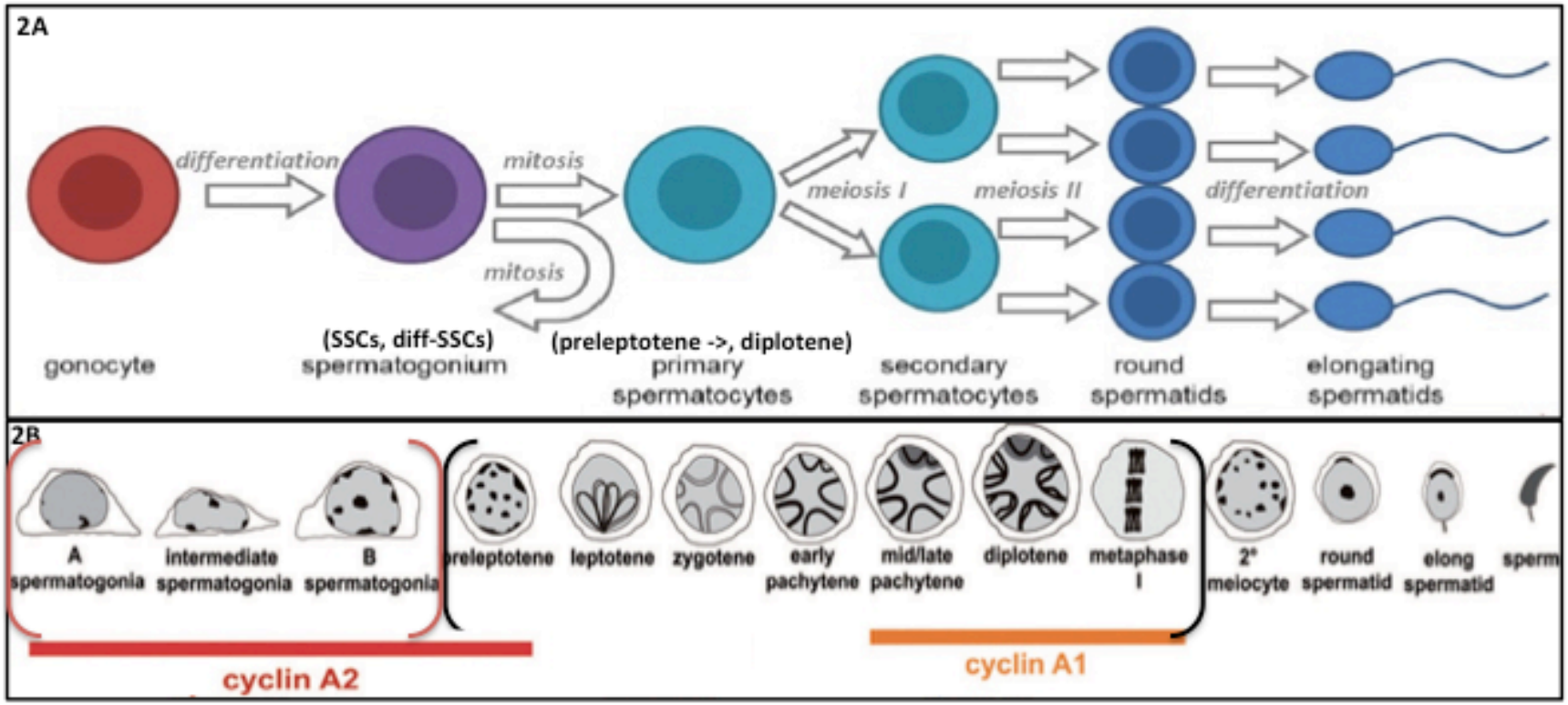

Figure 2: SSC Differentiation and A-type Cyclin niche in spermatogenesis. (A) Main Spermatogenic populations and differentiation scheme. Image obtained and modified from the Asian Journal of Andrology. (B) A-type *Cyclin* expression during spermatogenesis. According to the literature, *Ccna2* is expressed in the mitotic population as well as the preleptotene stage of spermatocyte differentiation. *Ccna1*, on the other hand, is expressed during the mid-pachytene stage up to the metaphase of Meiosis I. Differentiating SSCs (diff-SSCs) are shown enclosed in the red parentheses, while the stages of spermatocyte differentiation are enclosed in the black parentheses. Figure modified from Wolgemuth *et al*, 2008.

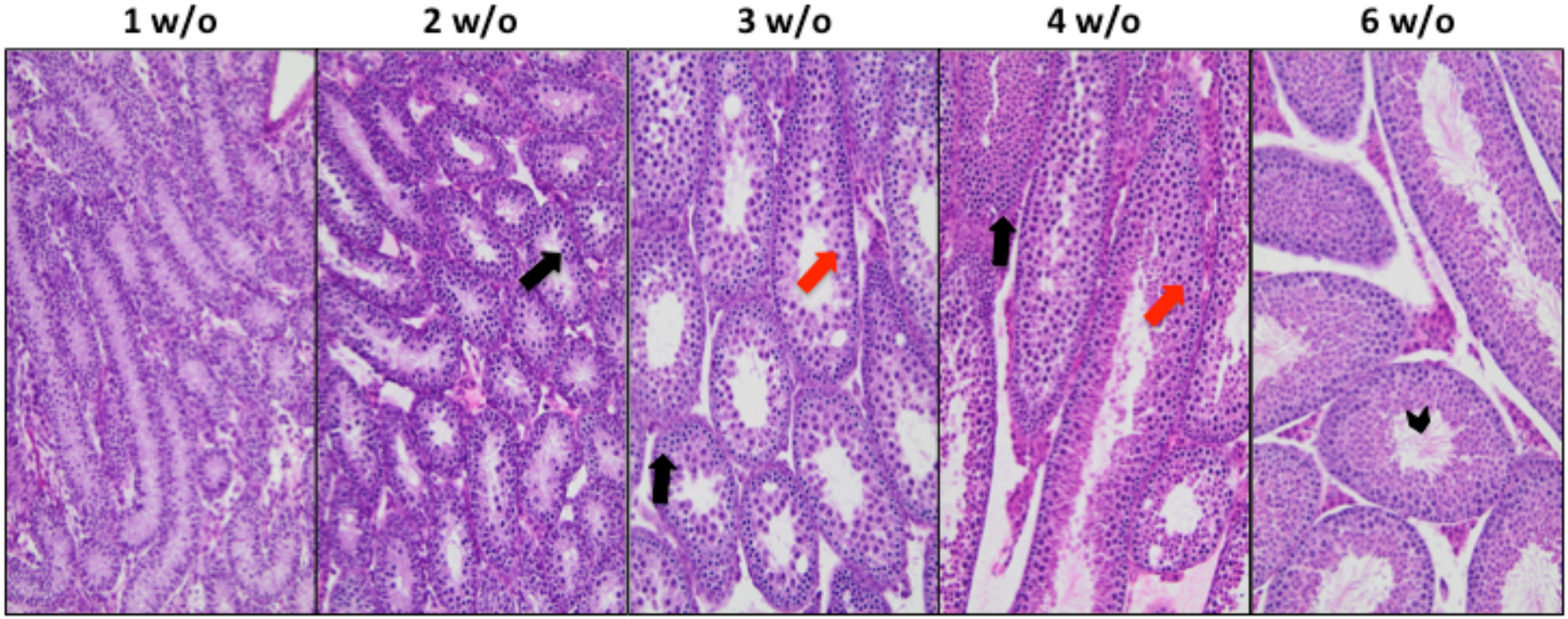

Figure 3: The 1st wave of spermatogenesis in wild-type mice (20x). During the 1st week, the tubules are still in the process of developing their lumen and consist mostly of SSCs and diff-SSCs. At 2 weeks old (w/o), tubules are at the zygotene stage (black arrow); at 3 w/o, at the diplotene stage (red arrow). Finally, spermatids begin to elongate around week 4 and sperm tails become visible in the lumen. By 6 w/o, the 1st wave has culminated, as seen in the numerous sperm tails present in the lumen (black arrowhead).

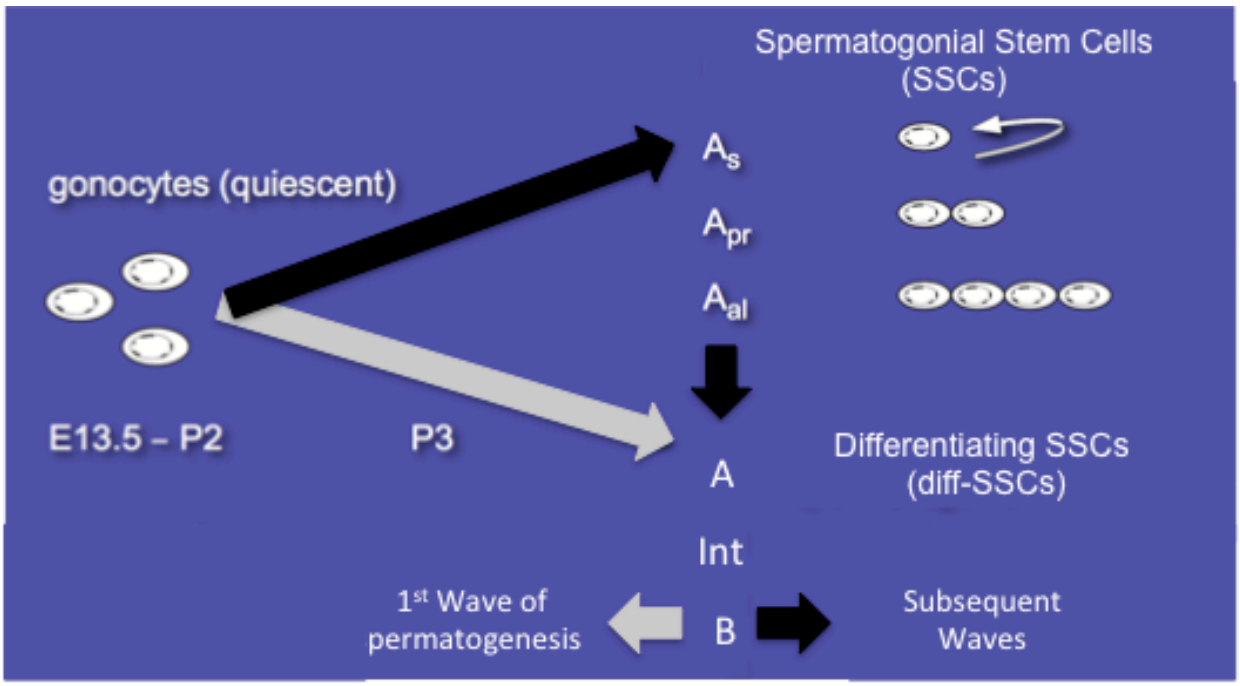

Figure 4: Asymmetric differentiation of gonocytes during the 1st wave of spermatogenesis. The 1st wave of spermatogenesis is characterized by the gonocytes' direct differentiation to A-type spermatogonia (diff-SSCs), which skip the SSC fate (PLZF-positive) and go directly into spermatogenesis (gray arrows). Once the gonocyte population has completely differentiated either into SSCs or diff-SSC's, the subsequent waves originate from the SSC population (black arrows). Figure obtained and modified from Payne, 2013.

C. Cyclin A2 Promoter Mutants

To evaluate the importance of E2F-mediated regulation of *Ccna2 in vivo*, we generated a mouse line with a knock-in mutation at the E2F binding site in its promoter along with another mouse line as a control (Figure 5). Although mice are viable and appear healthy, we observed infertility and early testicular atrophy in males homozygous for the promoter mutation.

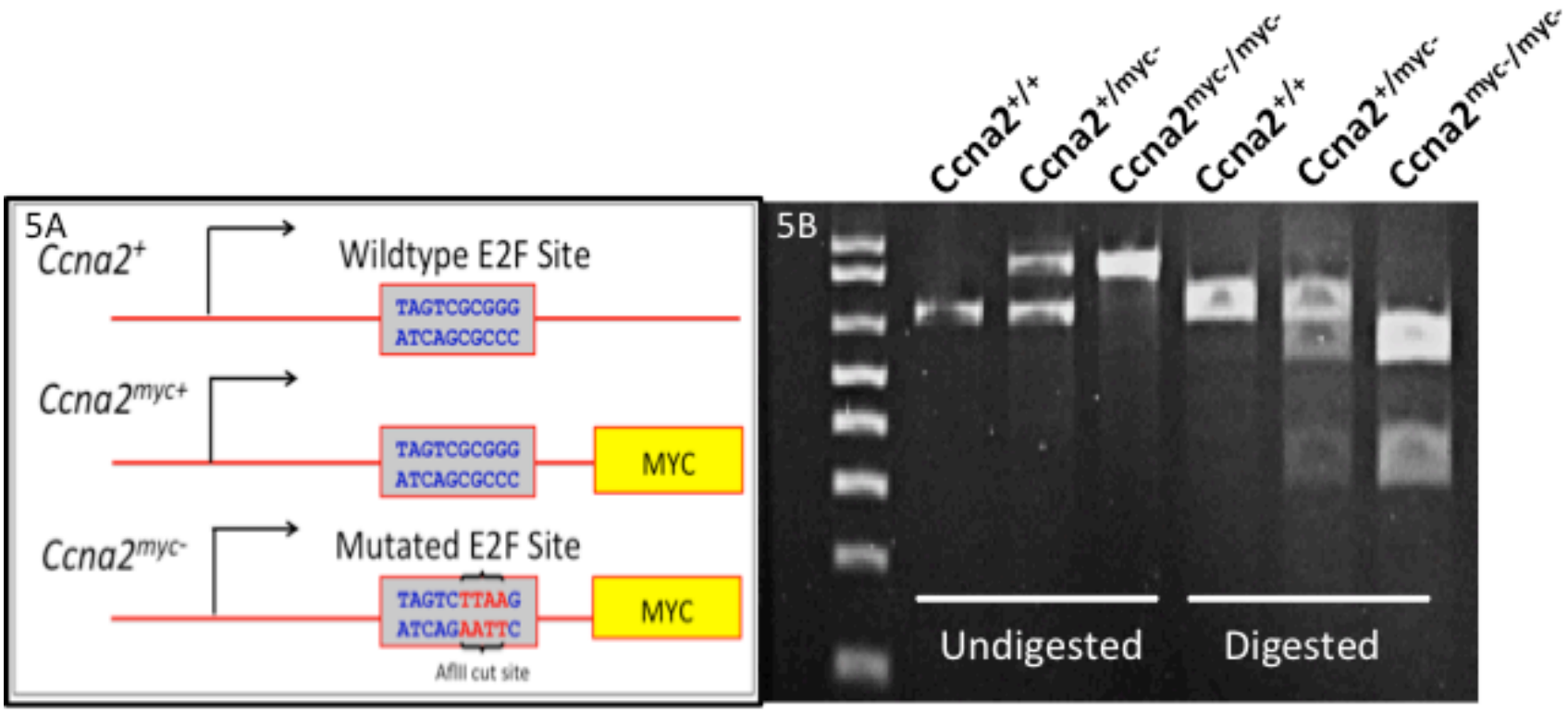

Figure 5: Generated alleles. (**A**) The wildtype locus of *Ccna2* (*Ccna2*$^{+}$) has its canonical E2F site 11 base pairs downstream of the transcription start site. The generated *Ccna2*$^{myc-}$ allele has a null E2F site with an AflII cut site for genotype verification (red) and a 5xMYC tag after the ATG translation start site. The *Ccna2*$^{myc+}$ allele, which was used as a control, has the wildtype E2F site and the 5xMYC tag. (**B**) Confirming the promoter mutation with restriction enzyme digestion for genotype verification. The MYC-tagged alleles have a PCR product (~850bp) that is much larger than the *Ccna2*$^{+}$ allele (~650bp). When digested, the *Ccna2*$^{myc-}$ PCR product partitions into two bands (~300bp, 550bp), confirming the presence of the promoter mutation.

II. **Hypothesis**

The promoter mutation's isolated effect on meiosis and CDK2's specialized role in this process suggests that misregulation of *Ccna2* expression due to loss of E2F binding interrupts proper CDK2 activity in meiosis. This hinders production of viable sperm and confers infertility in males homozygous for the promoter mutation.

III. **Aims**

Aim 1: Characterize the early testicular atrophy observed in *Ccna2*$^{myc-/myc-}$ males.

1A. Establish at what point in development the testes begin to atrophy.

1B. Diagnose the subcellular population(s) that are affected by the mutation.

Aim 2: Evaluate the changes in *Ccna2* expression and localization throughout development caused by the promoter mutation.

2A. Measure relative *Ccna2* expression levels throughout development.

2B. Quantify the CCNA2-positive cell populations and analyze potential fluctuations in their numbers.

Aim 3: Establish the source of the phenotype and what role of CCNA2 is being impaired

3A. Verify the mitotic activity of the stem cell population

3B. Assess one of the known roles of CCNA2/CDK2 like DNA Double Strand Break induction and how it is affected by the promoter mutation.

IV. **Methods**

Tissue Collection: Male mice were harvested at 1, 2, 3, 4, 6 and 12 weeks of age. Testes were weighed and either frozen in liquid Nitrogen for RNA extraction, fixed in bouin's for histological analysis (24 hours) or in formalin (48 hours) for immunohistochemical/ immunofluorescence assays (IHC/IFC).

cDNA preparation: Whole testes were homogenized and RNA was isolated with TriZol. Nucleic acid concentration was quantified with the Nanodrop spectrophotometer and cDNA was prepared using reverse transcriptase.

Real-time PCR (qPCR): RNA was extracted from mice heterozygous for each generated allele (*Ccna2*$^{+/myc+}$, *Ccna2*$^{+/myc-}$) and MYC-specific primers were designed to amplify only the myc-tagged *Ccna2* alleles (*Ccna2*$^{myc+}$, *Ccna2*$^{myc-}$).

Slide Preparation: Dissected tissues were fixed in 10% neutral-buffered formalin solution for 48 hours and transferred to 70% ethanol. Tissues were processed, embedded in paraffin, cut in 5µm sections on positively charged slides, de-paraffinized, rehydrated, and stained with H&E. For IHC/IF experiments and quantifications, three biological replicates (n=3) were included per stained slide.

Immunohistochemistry (IHC): Formalin-fixed testes sections were stained using a Bond Rx autostainer (Leica). Briefly, slides were baked at 65^{o}C for 15min and the automated system performed dewaxing, rehydration, antigen retrieval, blocking, primary antibody incubation, post primary antibody incubation, detection (DAB), and counterstaining using Bond reagents (Leica). Samples were then removed from the machine, dehydrated through ethanol and xylenes, mounted and coverslipped. These were stained for phosho-yH2AX (p-yH2AX) to assess levels of DSB induction and repair. Antigen retrieval and antibody concentration can be found in Supplemental Table 1.

Immunofluorescence (IF): Formalin-fixed testes sections were stained with anti-MYC (CCNA2) and anti-PLZF (SSC marker); nuclei were visualized by staining with DAPI. Thesee were then mounted with aqueous mounting media. Antibody concentrations can be found in Supplemental Table 1.

Quantification of IHC/IF stains: The Vectra Analysis System was used to image and take 40x pictures of the three testicular sections of biological replicates in the IHC/IF stained testes sections. All of the pictures from biological replicates were combined, and those images that had fixing, staining or mounting artifacts or contained portions of the epididymis were excluded from further analyses. The inForm Image Analysis software was then used to analyze the captured images by generating algorithms trained to quantify and analyze the intensity and localization of the p-yH2AX, MYC and PLZF markers. A description of these algorithms can be found in Supplemental Table 2. The analyzed images were reviewed to ensure that the trained algorithms performed proper nuclear segmentation and marker-positivity detection. Data from the images of biological replicates were then combined and were subjected to rank order analysis using a non-parametric model of quartile analysis.

V. **Results**

Testicular atrophy begins around the 3nd week of age and progresses throughout adulthood.

Measured testicular weights begin showing a significant deviation of testicular mass between the control lines (*Ccna2*$^{+/+}$/*Ccna2*$^{myc+/myc+}$) and the promoter mutant line starting at the 3 w/o time point; this difference persists throughout the rest of the measured time points and represents a 3-fold decrease in testicular mass in *Ccna2*$^{myc-/myc-}$ (Figure 6). The *Ccna2*$^{+/+}$ and *Ccna2*$^{myc+/myc+}$ lines also have a subtle difference in weights, with a 1.2-fold decrease of testicular mass in the *Ccna2*$^{myc+/myc+}$ adults. This data reveals a spermatogenic defect that begins during the 1st wave of spermatogenesis and persists in subsequent waves, causing *Ccna2*$^{myc-/myc-}$ testes to atrophy early in development.

Promoter mutants are unable to complete the 1st wave of spermatogenesis and undergo severe loss of spermatogenic populations.

Histological analysis of *Ccna2*$^{myc/myc-}$ tubules (Figure 7) showed a delay in spermatogenesis at 2 w/o, when developing spermatocytes only reach the preleptotene stage while the control lines are at the zygotene stage of spermatid differentiation. This is followed by a progressive degeneration of the differentiating cell populations in the seminiferous tubules from 3 to 4 w/o. At 3 weeks, the seminiferous tubules of control lines have reached the Diplotene stage, while a few of those from *Ccna2*$^{myc-/myc-}$ mice have pachytene spermatocytes; the others are completely depleted of these. At 4 weeks, promoter mutant tubules have almost completely lost all of the spermatogenic populations except for Sertoli Cells and SSCs. Surprisingly, *Ccna2*$^{myc-/myc-}$ seminiferous tubules begin to recover at 6 w/o and reach the pachytene stage. This repopulation coincides with the end of the 1st wave of spermatogenesis and the beginning of the adult program. 12 w/o *Ccna2*$^{myc-/myc-}$ males have multiple Sertoli cell-only tubules, as well as tubules with developing spermatids (surviving tubules). These remaining cell populations, however, do not rescue fertility nor do they

compensate for the lost testicular weight that occurs in the promoter mutants, meaning that spermatogenesis is still compromised. These data suggests that the promoter mutation is affecting the 1st wave of spermatogenesis and the subsequent ones differently, as seen in the surviving tubules that reach later stages of meiosis compared to those in the 1st wave.

Promoter mutants display an aberrant Ccna2 expression profile

Real-time PCR (qPCR) was performed on extracted RNA from males heterozygous for each myc-tagged allele (*Ccna2*$^{+/myc+}$, *Ccna2*$^{+/myc-}$) to assess the changes in *Ccna2* expression caused by the promoter mutation and not by the severe loss of spermatogenic populations (Figure 8). This analysis revealed an inverted profile of *Ccna2* expression throughout the 1st wave of spermatogenesis and after, a steady overexpression of transcription relative to the control groups. During the 1st week, *Ccna2*$^{myc-}$ expression is almost a two-fold lower compared to the *Ccna2*$^{myc+}$ allele, and both groups follow the same downregulatory trend into the 2nd week. However, transcription of the *Ccna2*$^{myc-}$ allele suddenly increases during the 3rd and 4th week, and is followed by a baseline level of overexpression that persists through adulthood and that is still higher than *Ccna2*$^{myc+}$ levels of expression. The expression of *Ccna1* was also measured (Supplemental Fig. 1) in order confirm that it was not being upregulated to compensate for *Ccna2*'s lack of expression, since they have both been shown to share targets when bound to their corresponding catalytic *cdks* (Yang *et al.*, 1999). *Ccna1* expression was seen in 4 w/o *Ccna2*$^{+/+}$ mice, but not in 4 w/o *Ccna2*$^{myc-/myc-}$, suggesting that the stage of its expression had not been reached yet in the promoter mutants and no upregulation was occurring to compensate for the lack of *Ccna2* expression.

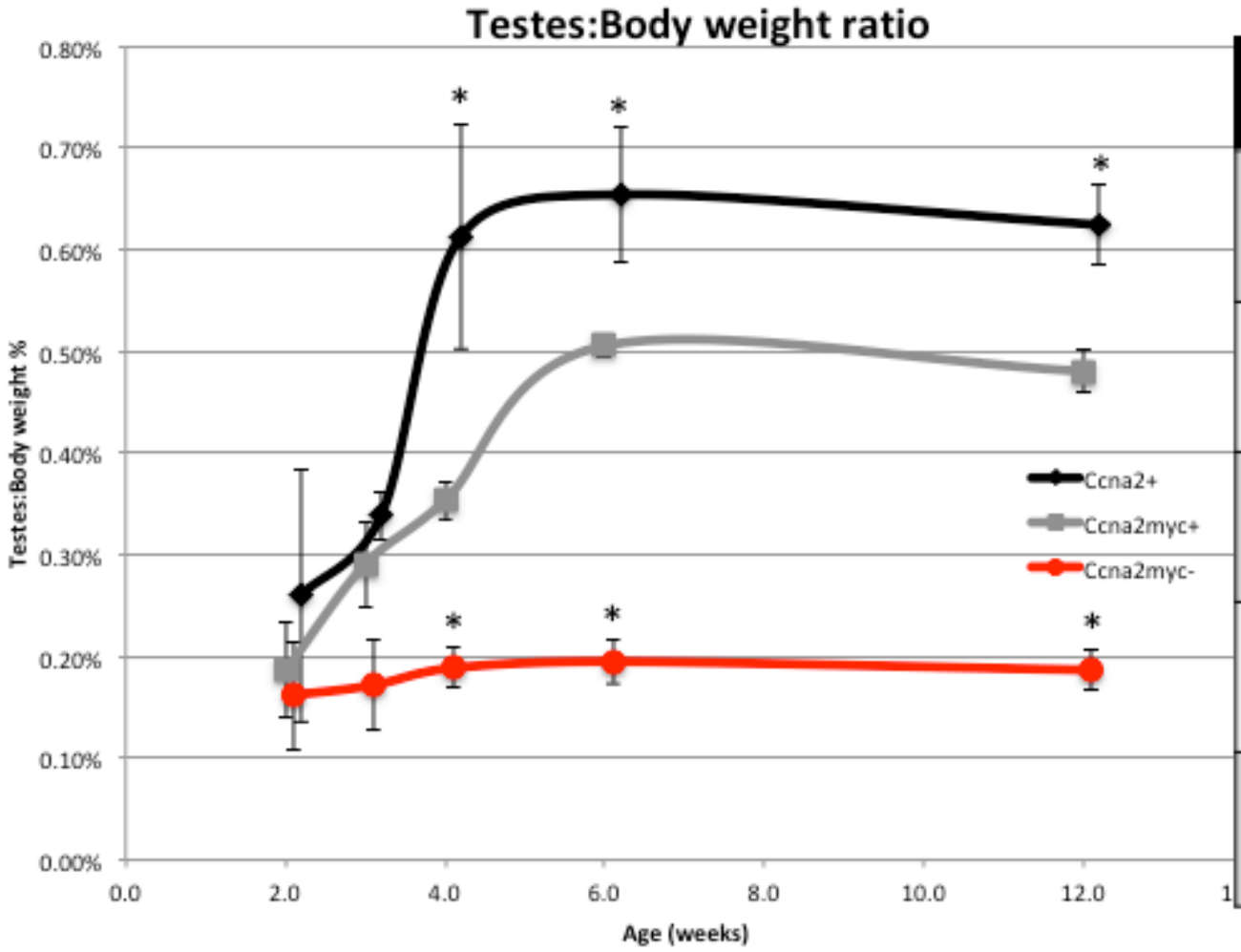

Time point	Genotype	Avg testes:body wt ratio
2 w/o	Ccna2+	0.26% (n=5)
	$Ccna2^{myc+}$	0.19% (n=4)
	$Ccna2^{myc-}$	0.16% (n=5)
3 w/o	Ccna2+	0.34% (n=5)
	$Ccna2^{myc+}$	0.29% (n=4)
	$Ccna2^{myc-}$	0.17% (n=5)
4 w/o	Ccna2+	0.61% (n=6)
	$Ccna2^{myc+}$	0.35% (n=5)
	$Ccna2^{myc-}$	0.19% (n=6)
6 w/o	Ccna2+	0.65% (n=5)
	$Ccna2^{myc+}$	0.51% (n=6)
	$Ccna2^{myc-}$	0.20% (n=4)
12 w/o	Ccna2+	0.62% (n =5)
	$Ccna2^{myc+}$	0.48% (n=4)
	$Ccna2^{myc-}$	0.19% (n=5)

Figure 6: Assessment of testicular atrophy. Testicular weights were normalized with body weight and compared across homozygotes of each experimental line. At adulthood, a 3-fold decrease in testicular mass is observed between the promoter mutants ($Ccna2^{myc-/myc-}$) and the wildtype line ($Ccna2^{+/+}$). Interestingly, the control lines also have a significant difference in testicular mass (1.2-fold decrease). Asterisk (*) signifies p-value of < 0.001 relative to the $Ccna2^{myc+/myc+}$ time point equivalent of each data point.

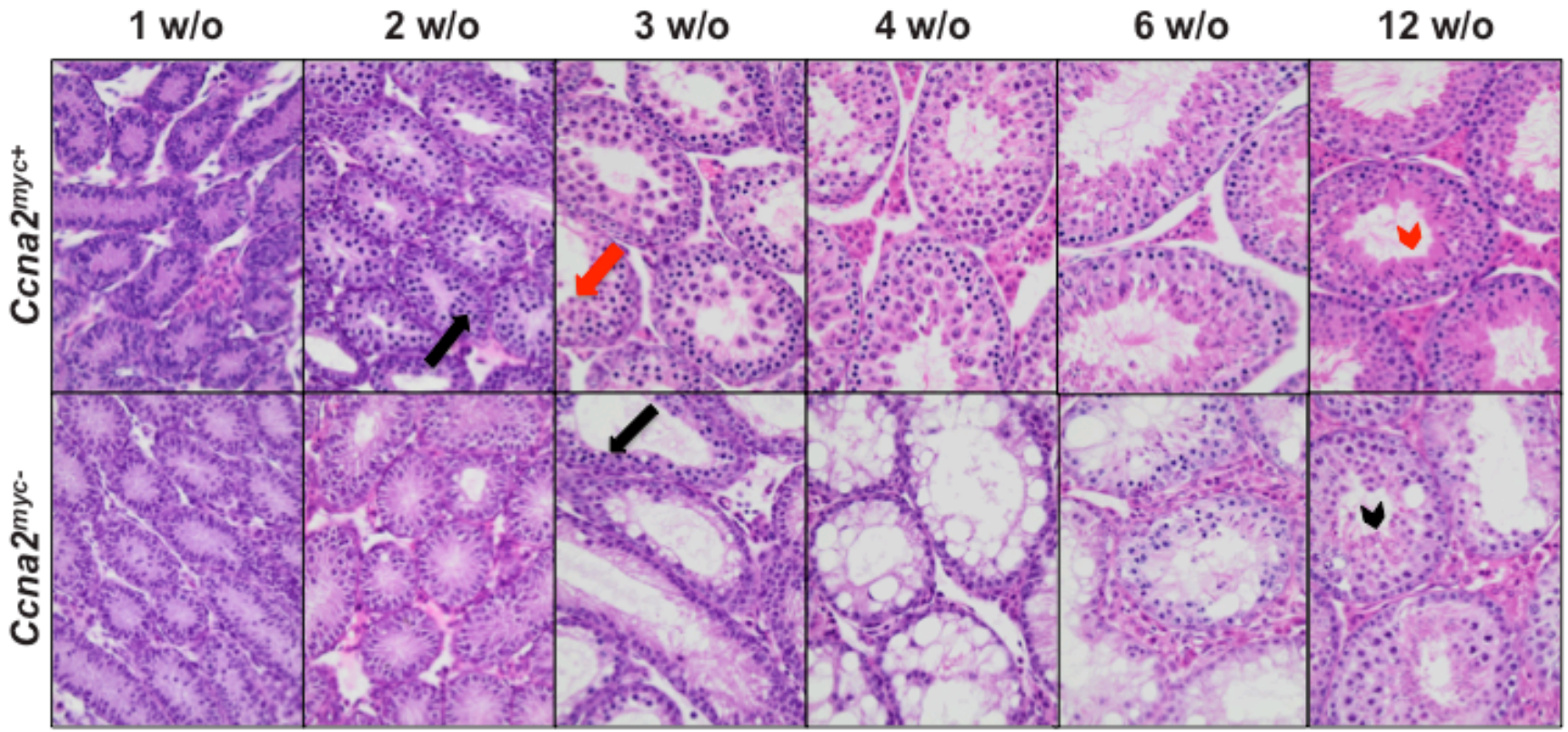

Fig 7: *Ccna2*$^{myc-/myc-}$ testes have a defective 1st wave of spermatogenesis: H&E-stained sections of bouins-fixed testes (40x). Spermatogonial populations appear to be normal at 1 w/o between the two groups. At 2 w/o, the control's seminiferous tubules have Zygotene spermatocytes (black arrows), which are absent in *Ccna2*$^{myc-/myc-}$ mutants until the 3 w/o time point. At 3 w/o, the control line has reached the pachytene stage (red arrows) while promoter mutants mutants undergo a progressive loss of differentiating cell populations that peaks at 4 w/o. The severe vacuolization observed in *Ccna2*$^{myc-/myc-}$ tubules corresponds to the empty pockets in the cytoplasm of the sertoli cells where spermatids usually reside. *Ccna2*$^{myc-/myc-}$ tubules partially recover their cell populations after the 1st wave of spermatogenesis (6 w/o-12 w/o), with some being positive for elongating spermatids (black arrowhead). These, however, do not show adequate sperm accumulation in the lumen like the control line (red arrowhead).

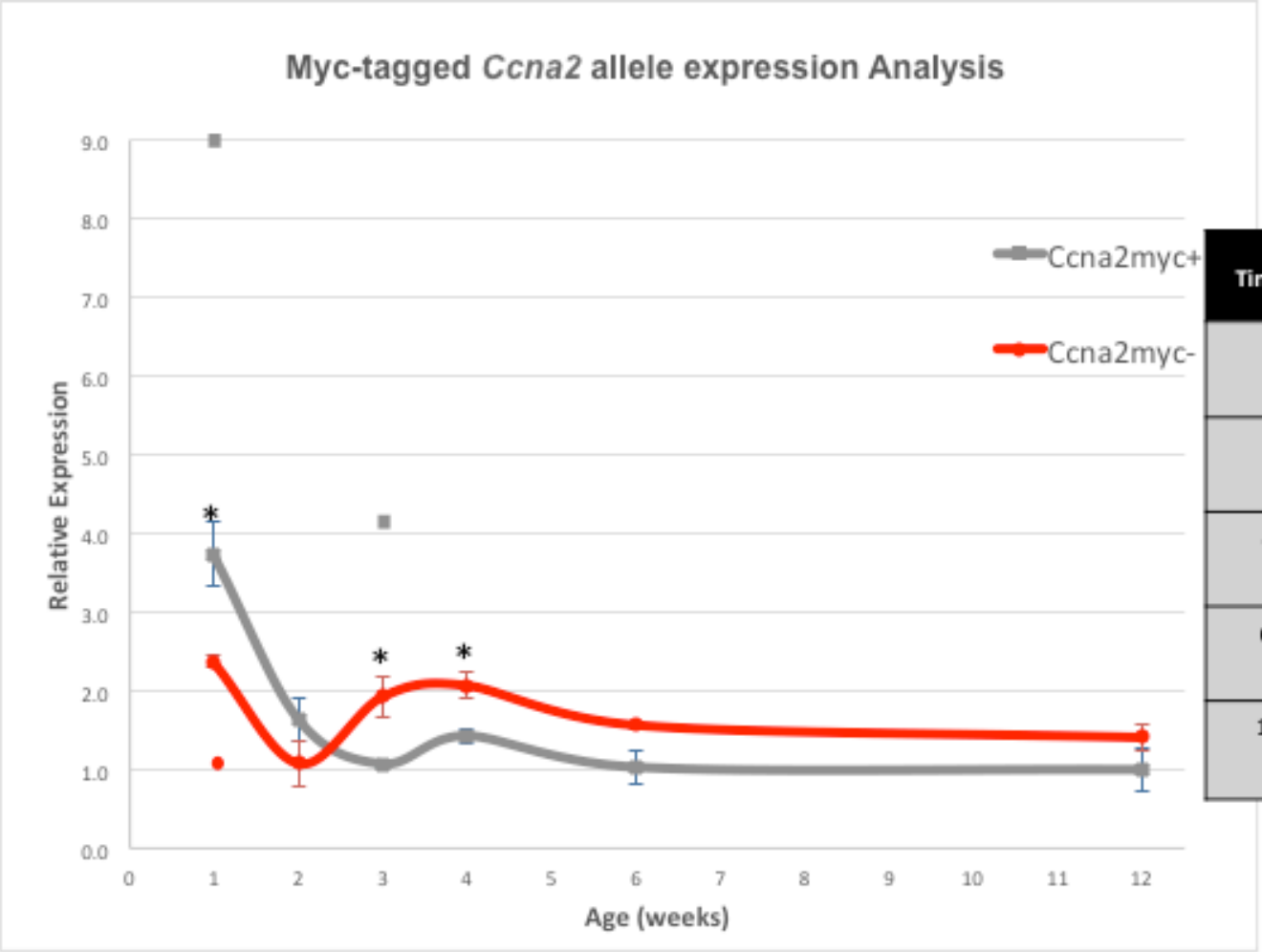

Time point	Genotype	Avg Relative expression
2 w/o	$Ccna2^{myc+}$	3.7 (n =4)
	$Ccna2^{myc-}$	2.4 (n=4)
3 w/o	$Ccna2^{myc+}$	1.6 (n=3)
	$Ccna2^{myc-}$	1.1 (n=3)
4 w/o	$Ccna2^{myc+}$	1.1 (n=4)
	$Ccna2^{myc-}$	1.9 (n=4)
6 w/o	$Ccna2^{myc+}$	1.4 (n=4)
	$Ccna2^{myc-}$	2.1 (n=4)
12 w/o	$Ccna2^{myc+}$	1.0 (n=4)
	$Ccna2^{myc-}$	1.6 (n=4)

Figure 8: Relative *Ccna2* expression analysis via qPCR. The $Ccna2^{myc-}$ allele's expression is inverted relative to the control. It shows lower levels of expression during the proliferative phase of the tubules (1 w/o) and elevated expression in adulthood, where SSCs are mostly quiescent. This upregulation of expression occurs after the 2 w/o time point, when the initial spermatogenic delay is observed. Data points were considered outliers if they fell outside a +/- 1 range from the extremes of the other values; these are depicted as single points and were not included in average or standard error calculations. Asterisk (*) represents a p-value of < .05 between genotypes of the same time point.

CCNA2 is found up to pachytene spermatocytes in the Ccna2$^{myc-/myc-}$ and Ccna2$^{myc+/myc+}$ mouse lines, an unforeseen localization of the protein in spermatogenesis

Immunofluorescent co-stains specific for the MYC-tag and PLZF (SSC marker) were used to study the mutation's effect on the stem cell populations and CCNA2's specific localization in spermatogenesis; since the wild-type *Ccna2* locus does not have a MYC-tag coding sequence, the corresponding mouse line was not used for this experiment. The literature has reported preleptotene spermatocytes as the last stage in spermatogenesis that sees CCNA2 expression (Wolgemuth, 2011), but these IF stains show CCNA2 expression in both zygotene and pachytene spermatocytes in both myc-tagged lines (Figure 9).

Promoter mutants have an increased number of cells with high CCNA2 levels

To see if the abnormal expression profile described by the qPCR experiment was reproducible at the cell population level, cells with high CCNA2 signal were quantified using the InForm Algorithm #1 (Table 2). The total number of cells per image was quantified for each genotype and time point (Figure 10). According to the data, there are no significant differences across the time points of the 1st wave of spermatogenesis, but those corresponding to subsequent waves (6 and 12 w/o) show that *Ccna2$^{myc-/myc-}$* tubules have fewer cells relative to the *Ccna2$^{myc+/myc+}$* control. To calculate the total number of cells with high CCNA2 signal (MYC^{++}) per image, the fraction of MYC^{++} cells calculated with Algorithm #1 was multiplied by the total number of cells (Figure 11). Interestingly, the data corresponding to the *Ccna2$^{myc-/myc-}$* mice appears to recapitulate the expression profile of the *Ccna2^{myc-}* allele throughout the 1st wave of spermatogenesis, with significantly lower levels of MYC^{++} cells at 2 w/o followed by a sudden increase in their numbers at 3 w/o and persistent higher levels of these relative to the control throughout the rest of the time points.

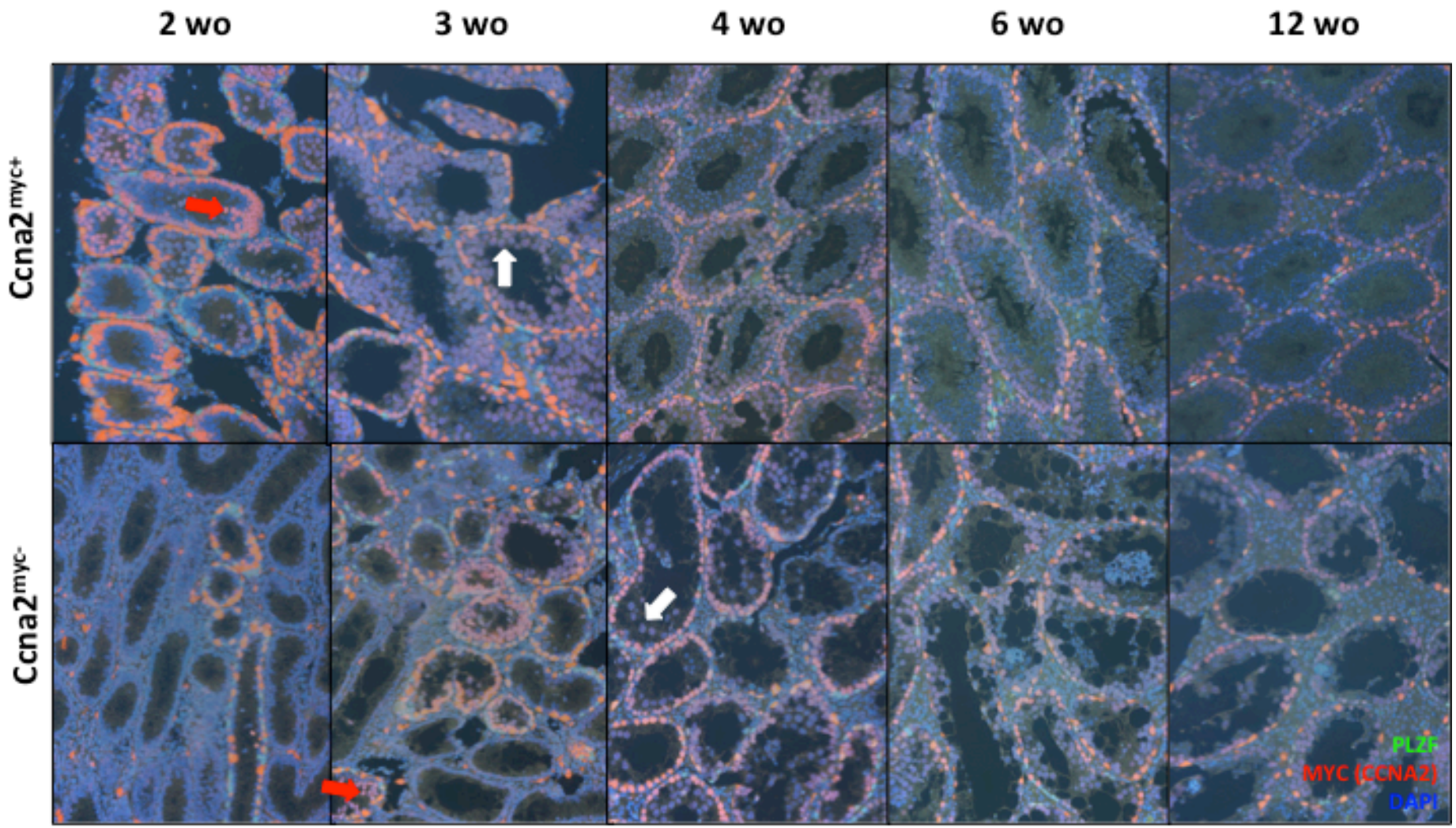

Figure 9: IF analysis of SSCs (PLZF-positive) and CCNA2-positive (MYC-positive) populations in the seminiferous tubules (40x). The sensitivity of the MYC-tag antibody allowed for very precise detection of CCNA2 protein in spermatogenic populations. This revealed an unforeseen presence of CCNA2 in zygotene (red arrow) and pachytene (white arrow) spermatocytes in both the *Ccna2*$^{myc-}$ and the *Ccna2*$^{myc+}$ lines.

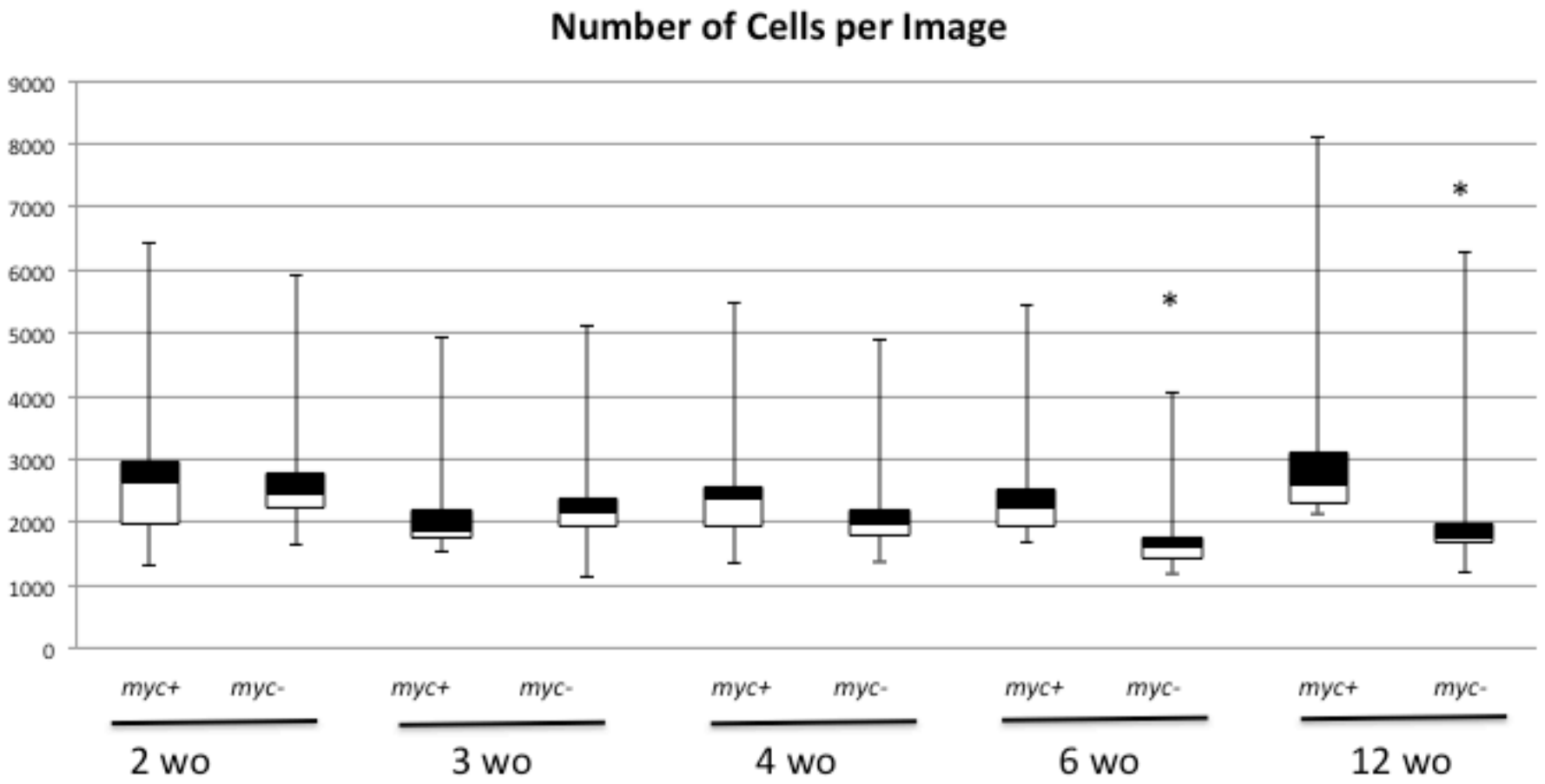

Figure 10: Total cell population quantification. Using Algorithm #1, the total number of cells per picture was quantified, images of biological replicates were combined and the data was subjected to quartile analysis. According to the analysis, only the last two time points have a significant difference between genotypes. This high number of cells in 6 and 12 w/o *Ccna2*$^{myc+/myc+}$ relative to the promoter mutant tubules corresponds to the increased number of cells across the testes from proper spermatogenesis progression. (Asterisk (*) signifies a p value < .05)

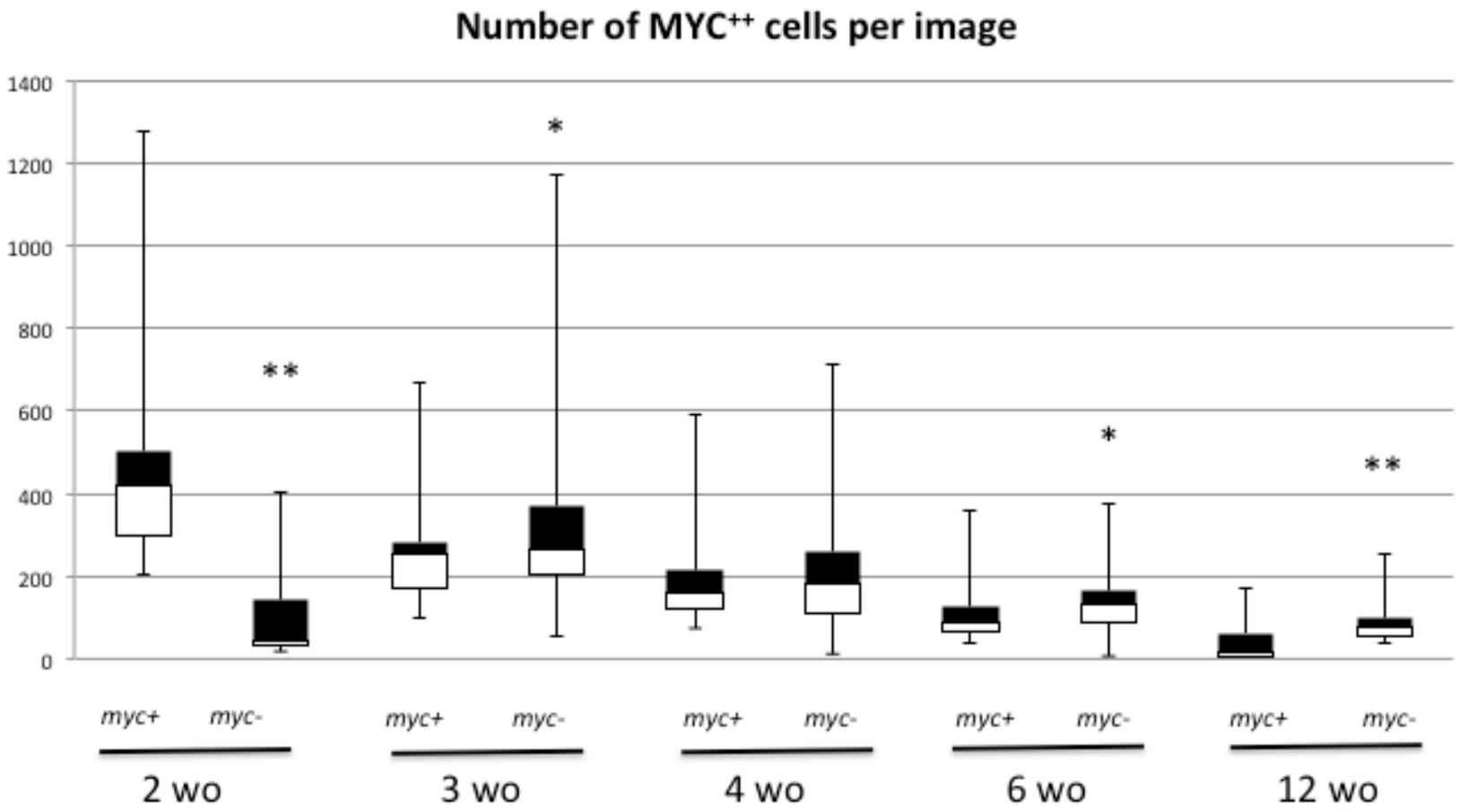

Figure 11: Stem Cell Population Analysis (SSCs and diff-SSCs). The fraction of MYC^{++} cells was calculated using Algorithm 1. Total number of stem cells expressing CCNA2 was calculated by multiplying the fraction of MYC^{++} cells by the total number of cells per image; all of the images of biological replicates were combined and subjected to quartile analysis. According to the data, all but the 4 w/o time points show significant differences across genotypes in the number of MYC^{++} cells per field. The *Ccna2*$^{myc-/myc-}$ testes have significantly lower MYC^{++} cells per field relative to the control at 2 w/o, and significantly elevated amounts at the 3, 6 and 12 w/o time points. (Single (*) and double (**) asterisks signify a p value of < .05 and < .005, respectively)

Ccna2$^{myc-/myc-}$ SSC expansion is delayed during the 1st wave of spermatogenesis but is then upregulated in subsequent waves.

Immunofluorescent PLZF and MYC co-stains were analyzed with Algorithm #2 (Table 2) to study the SSC population and its proliferative activity. The total number of PLZF^{+} cells per image was quantified for each genotype and time point (Figure 12). Then, the fraction of PLZF^{+}/MYC^{++} cells calculated with Algorithm #2 was multiplied by the total number of PLZF^{+} cells per image (Figure 13). According to this analysis, there appears to be a slight increase in PLZF^{+} cells in adult *Ccna2$^{myc-/myc-}$* males. However, an even more pronounced increase is observed in the number of PLZF^{+}/CCNA2^{++} cells after the 2 w/o time point in *Ccna2$^{myc-/myc-}$* tubules compared to those from the control line, suggesting an increased fraction of SSCs that are cycling in promoter mutant tubules. As a whole, this data suggests an upregulation of stem cell presence and activity in *Ccna2$^{myc-/myc-}$* tubules after the 2 w/o delay occurs, especially compared to the quiescent state of SSCs in 12 w/o *Ccna2$^{myc+/myc+}$* testes.

Surviving seminiferous tubules of promoter mutants show a delay in DSB induction during the 1st wave of spermatogenesis.

p-yH2AX stains for DNA damage assessment confirmed that *Ccna2$^{myc-/myc-}$* male mice are able to induce DSBs for recombination during the 1st wave of spermatogenesis, but tubules are either delayed in doing so or are negative for DNA damage, indicating a complete vacancy of differentiating spermatocytes and the stem cell population (sertoli-cell only) (Figures 14 and 15). During the 2 w/o time point, a small fraction of *Ccna2$^{myc-/myc-}$* tubules begin to induce DSBs, but are nowhere close to the level of DSB induction seen in the control lines. Then, the non-sertoli cell-only tubules (surviving tubules) achieve high levels of DSBs during 3 w/o. Controls on the other hand already have pachytene spermatocytes, which have resolved all DSBs and are positive for p-yH2AX staining in the nuclear region of the sex body (Blanco, 2009). The p-yH2AX stain at the peak of degeneration is met with a

partial loss of the cells positive for high levels of unresolved DSBs, which then return at the 6 w/o time point and appear to be present in almost all surviving tubules.

Surviving tubules of adult promoter mutants appear to have a strong presence of cells with high levels of unresolved DSBs

Qualitative observation of 12 w/o *Ccna2*$^{myc-/myc-}$ testes stained with p-yH2AX (Figure 16) shows a subtle preference for dark-staining spermatocytes in the basal side of the tubules. Although the control lines also have these dark-staining cells, the frequency of occurrence across all of the tubules of the testis is less relative to the *Ccna2*$^{myc-/myc-}$ males, as seen in the 4x and 40x images of p-yH2AX stains of 12 w/o testes. Algorithm #3 (Supplemental Table 2) was used to quantify the total amount of these high p-yH2AX-positive cells (p-yH2AX^{++}) per image. However, the dark-staining elongating spermatocytes found in the control lines interfered with the exclusive quantification of cells that are shared between the controls and the promoter mutants, making the algorithm overestimate the number of p-yH2AX^{++} cells for *Ccna2*$^{+/+}$/*Ccna2*$^{myc+/myc+}$ lines at the 4, 6 and 12 w/o time points (Figure 17). This tendency will require further analysis and its quantification optimized for confirmation.

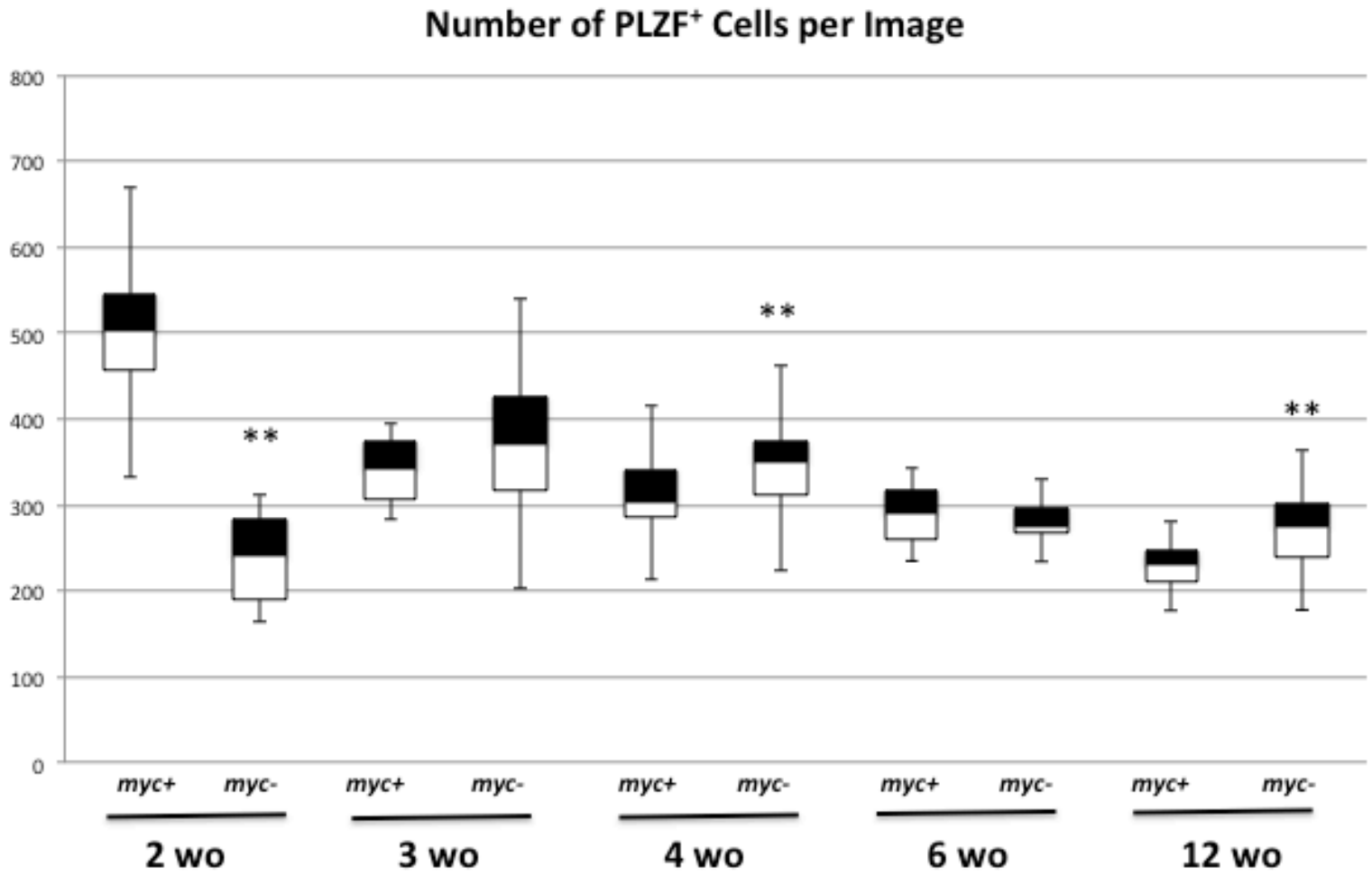

Figure 12: SSC Population Analysis. The total number of PLZF+ cells (SSCs) per image was calculated using Algorithm 2. Images of biological replicates were combined and subjected to quartile analysis. According to the data, there is a significantly lower amount of SSCs at 2 w/o in *Ccna2*$^{myc-/myc-}$ males, but then a significant increase of these at the 4 and 6 w/o time points. SSC population levels also appear to correlate with the *Ccna2*$^{myc-}$ allele expression profile. (Double (**) asterisks signify a p value of < .005 across genotypes of the specified time point)

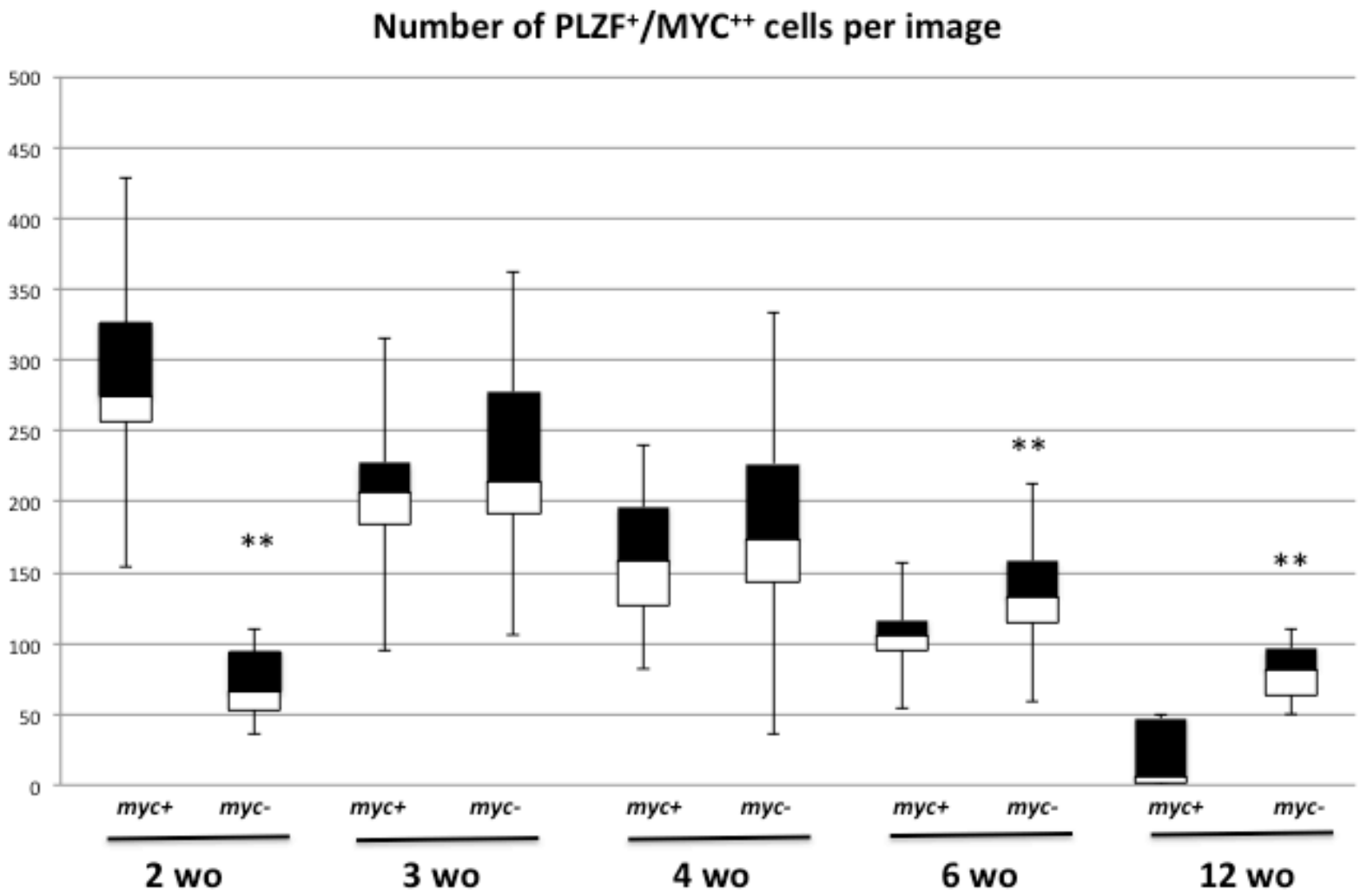

Figure 13: Cycling SSC Population Analysis. The total number of cycling SSCs cells (PLZF^{+}/MYC^{++}) per image was calculated by multiplying the total PLZF^{+} cells by the fraction of PLZF^{+}/MYC^{++}cells determined with Algorithm 2. Images of biological replicates were combined and subjected to quartile analysis. According to the data, there is a significantly higher number of SSCs cycling per image at 2 w/o in *Ccna2*$^{myc-/myc-}$ males, but then a significant increase of these at the 4 and 6 w/o time points. SSC population levels also appear to correlate with the *Ccna2*$^{myc-}$ allele expression profile. (Double asterisks (**) signify a p value of $< .005$)

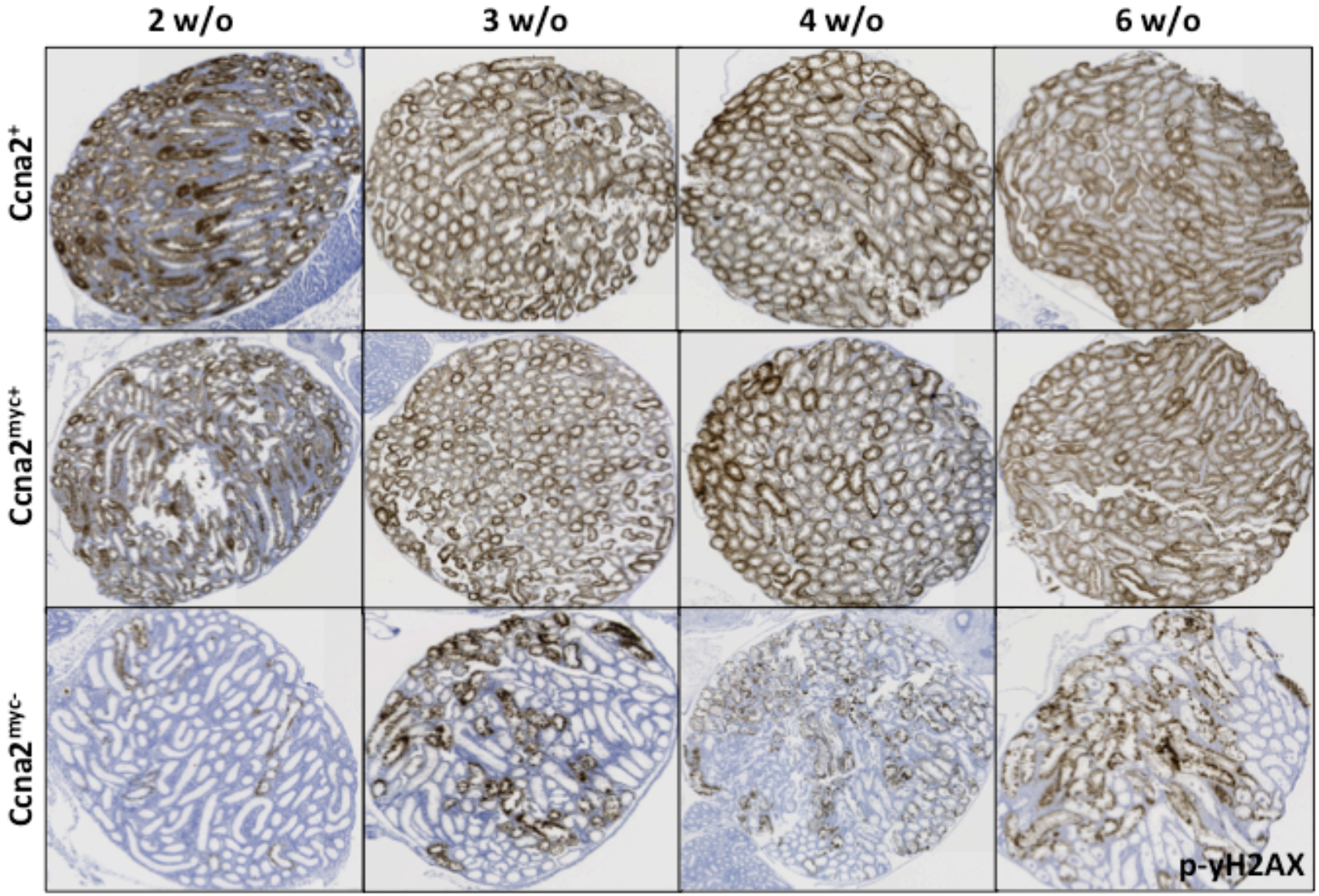

Figure 14: DSB induction and repair assessment during the 1st wave of spermatogenesis via p-γH2AX IHC stain (4x). *Ccna2*$^{myc-/myc-}$ tubules that are not sertoli-cell only show a delay in DSB induction relative to the control lines from 2 to 3 w/o. Then, these tubules lose part of the spermatid population that has high levels of DSBs during 4 w/o, the peak of histological degeneration. The population of high DSBs-containing spermatids reestablishes itself at 6 w/o and appears to occupy an unusually high number of surviving tubules.

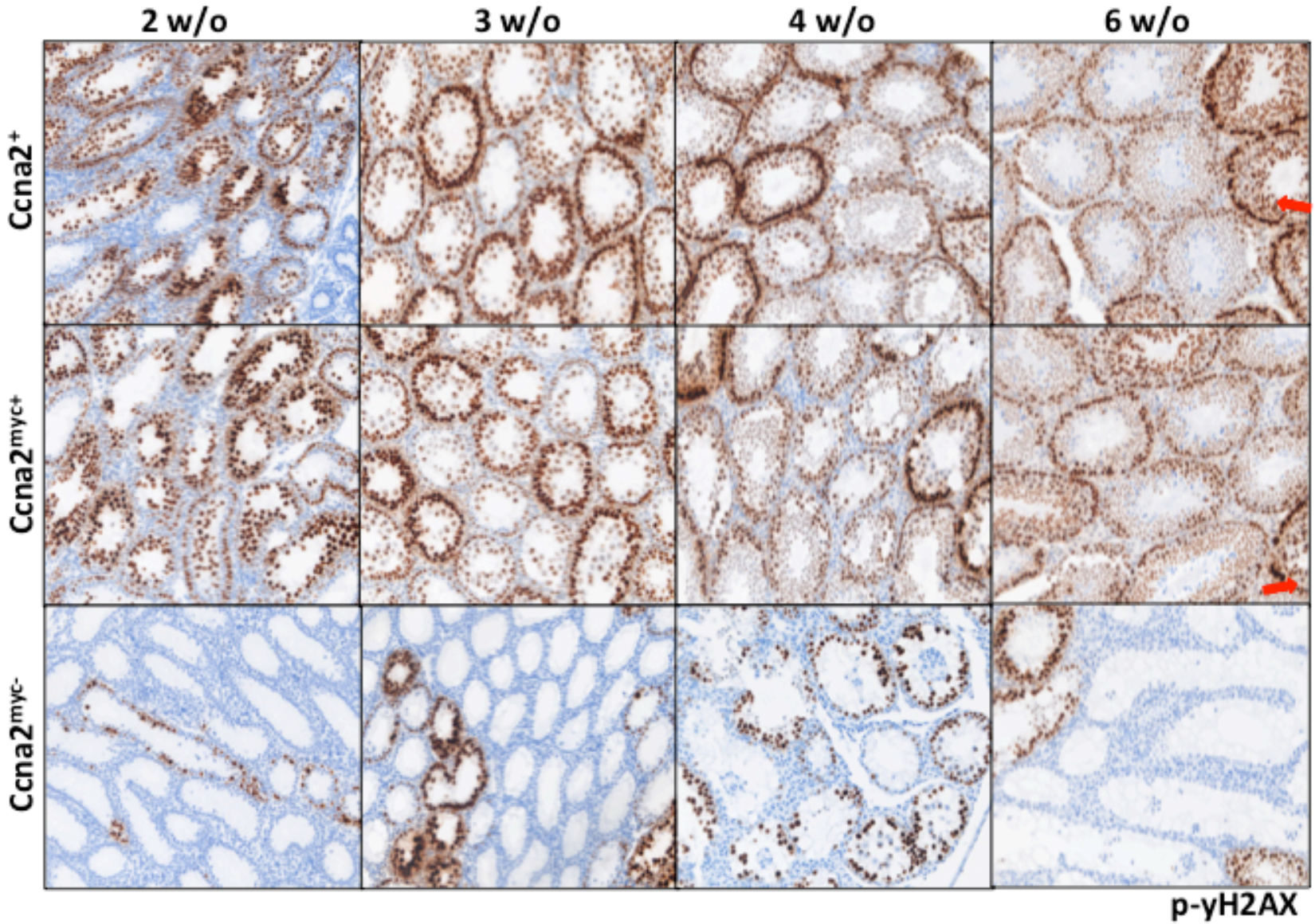

Figure 15: DSB induction and repair assessment via p-γH2AX IHC stain (40x). A closer look at the p-γH2AX stain reveals that most of the tubules that surviving tubules in promoter mutants only produce low amounts of spermatids with resolved DSBs. Elongating spermatids, which are almost completely absent in promoter mutant testes and interfered with proper quantification, are shown with red arrow.

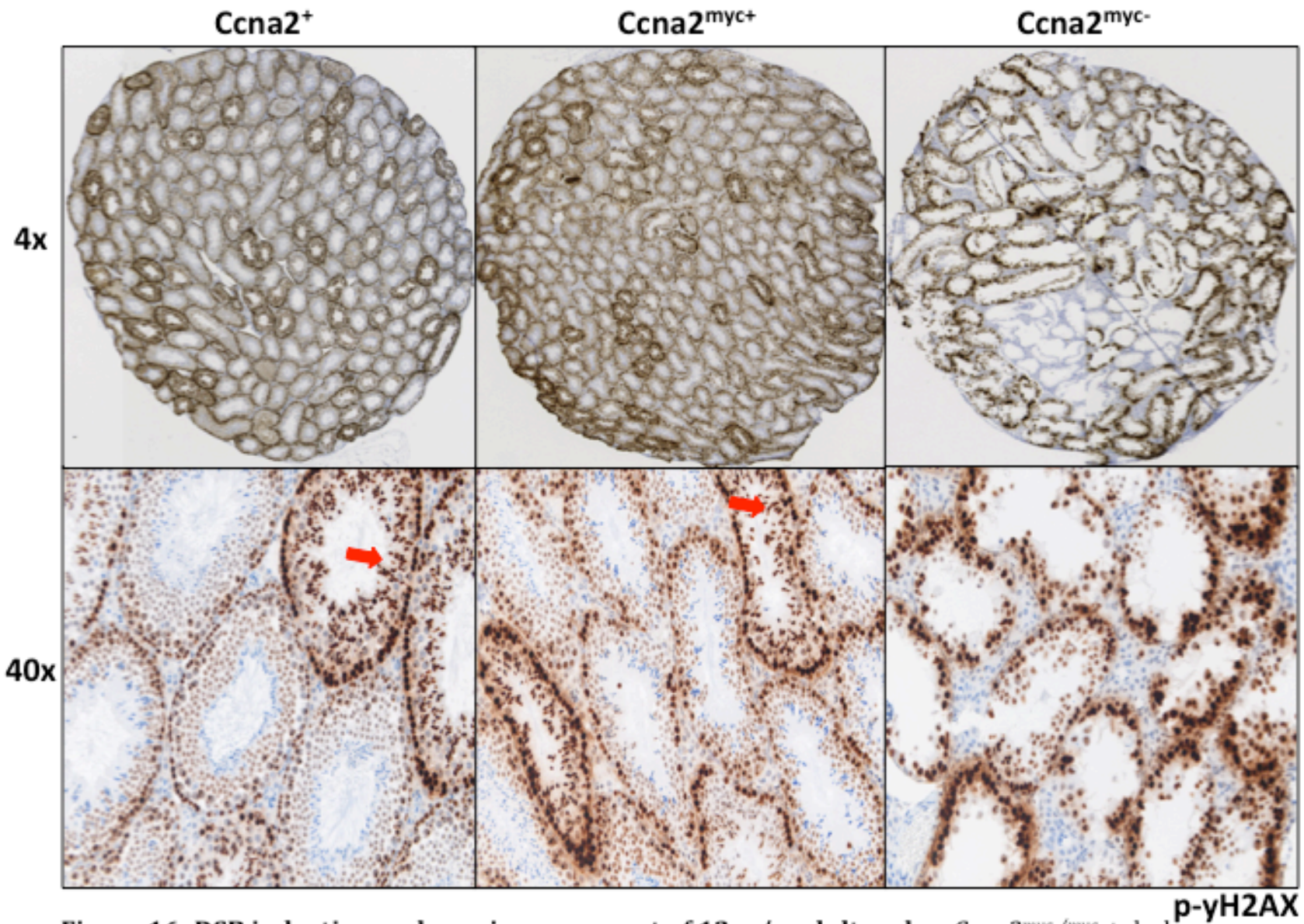

Figure 16: DSB induction and repair assessment of 12 w/o adult males. *Ccna2*$^{myc-/myc-}$ tubules appear to be predominantly populated by the cells with high DSBs, possibly suggesting a partial cellular arrest in spermatocytes that cannot resolve these. The dark-staining elongating spermatids in the control lines (red arrow) interfered with the quantification of these images using Algorithm #3 at this time point.

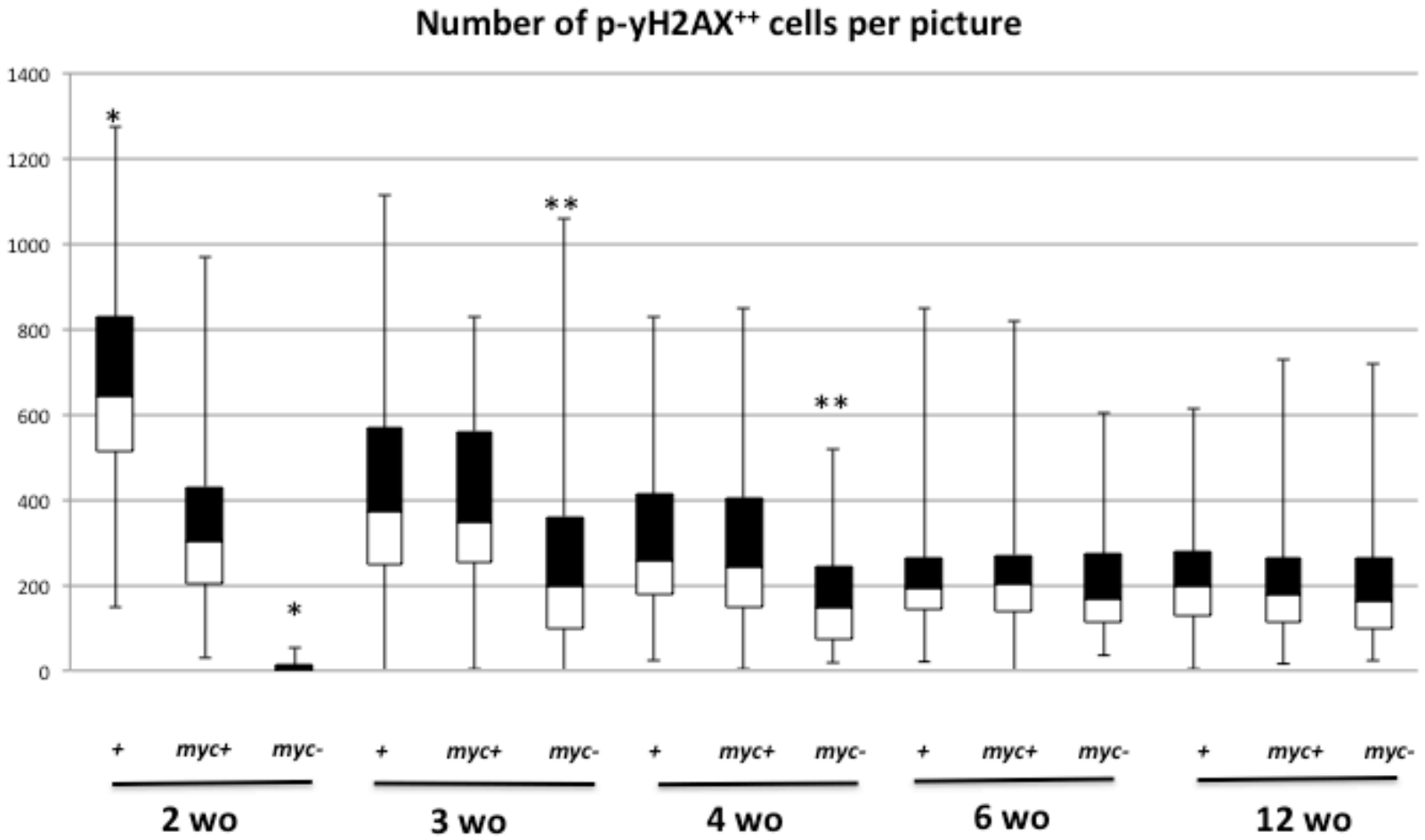

Figure 17: Quantitative Analysis of cells with high DSBs (p-yH2AX^{++}) per image. The total number of dark-staining p-yH2AX spermatocytes (p-yH2AX^{++}) per image was determined with Algorithm 3, then images of biological replicates were combined and subjected to quartile analysis. After careful evaluation of the image scoring performed by Algorithm 3, the established threshold was found to detect elongating spermatids at 4, 6 and 12 w/o as p-yH2AX^{++} spermatocytes. This population is not present in *Ccna2*$^{myc-/myc-}$ tubules, therefore the relative number of p-yH2AX^{++} spermatocytes in controls is overestimated at these time points. However, data corresponding to early stages of the 1st wave of spermatogenesis (2-3 w/o), where elongating spermatids still haven't appeared, is valid. Single (*) and double (**) asterisks indicate a p-value of $< .05$ and $< .005$, respectively, relative to the *Ccna2*$^{myc+/myc+}$ controls.

VI. **Discussion**

The knock-in mutation in the E2F binding site of *Ccna2's* promoter has caused a profound degeneration of spermatogenic populations, severely compromising the fertility of male *Ccna2*$^{myc-/myc-}$ mice and causing a three-fold decrease in testicular weight. The generated control line, *Ccna2*$^{myc+/myc+}$, also displays some subtle phenotypes that, even though are not anywhere close to those observed in the promoter mutant line, are worth discussing. The unexpected localization of CCNA2 protein in spermatocytes beyond the preleptotene stage in both myc-tagged lines could either represent a previously undescribed localization of the protein, or an interruption of *Ccna2* protein regulation caused by the myc-tag. The sensitivity of the MYC antibody could have allowed for a more precise detection of the protein, revealing this subtle presence of CCNA2 in zygotene and pachytene spermatocytes. However, the myc-tag could also be interfering with proper CCNA2 degradation, causing a small amount of the protein to be carried over later stages of spermatid differentiation. While the slight decrease in testes:body weight ratios and this novel localization of CCNA2 in spermatogenesis seen in *Ccna2*$^{myc+/myc+}$ mice might suggest that the myc-tag is interfering with CCNA2 protein folding/function and contributing slightly to the testicular atrophy phenotype, *Ccna2*$^{myc+/myc+}$ males are still fertile and progress through the 1st wave of spermatogenesis at the same pace as wild-type males. Therefore, they can be deemed a good control to study the consequences of the promoter mutation in *Ccna2* during sperm development. This slight decrease in *Ccna2*$^{myc+/myc+}$ testicular weights also highlights the important role CCNA2 plays in spermatogenesis, since a subtle alteration to the protein structure (and folding, potentially) causes a slight but significant reduction in testicular mass.

The complexity of the phenotype and the variable rate of degeneration across the seminiferous tubules of mutant testes demanded careful, objective and standardized methods to analyze both *Ccna2*$^{myc-}$ allelic expression and the performed IHC/IF stains. The qPCR experiment was designed to amplify the myc-tagged allele from RNA of mice heterozygous for *Ccna2*$^{myc+}$ or *Ccna2*$^{myc-}$ alleles. Since these heterozygous mice do not undergo testicular atrophy, the experiment allowed for the assessment of the mutation-

specific changes in transcription instead of the relative changes in *Ccna2* transcript levels caused by loss or absence of spermatogenic populations,. In the case of IHC/IF analyses, the Vectra imaging microscope and the inForm image analysis software offered a great platform to standardize the stain quantifications, and proved to be successful in generating results that were more reproducible compared to the typical visual appraisal methods not conducted through an instrument or algorithm; however, the platform isn't perfect and required arduous optimization. Due to the degenerative effect of the promoter mutation, cell population-analyzing algorithms had to be tailored so as to exclude those populations that are not shared between the experimental lines. Including these unshared populations in the analysis would underestimate the fraction of cells positive for the established thresholds, since control tubules have extremely high numbers of cells compared to the promoter mutants.

Proper normalization was achieved with the algorithms for the PLZF/CCNA2 stains, which were designed to compare shared spermatogenic populations and adjust the threshold for marker positivity according to the variations in staining intensity caused by exposure artifacts. Even though these algorithms did not account for the number of tubules or the amount of space corresponding to the lumen or the background of each image, reproducible data was generated and significant trends have been identified. Unfortunately, the p-yH2AX stain quantification saw interference from the elongating spermatid population, which displays intense p-yH2AX staining in the control groups but is barely present, if at all, in the *Ccna2*$^{myc-/myc-}$ tubules. For this reason, the qualitative observations from the p-yH2AX stain were not completely recapitulated with Algorithm #3, which will require further optimization if the stain is to be analyzed quantitatively.

The early testicular atrophy observed in *Ccna2*$^{myc-/myc-}$ testicular weights and the quick degeneration of their tubules during the first postnatal weeks indicates a defect in the 1st wave of spermatogenesis that persists throughout adulthood. Although the precise developmental time point at which *Ccna2* misregulation begins to affect proper cell cycle progression is yet unknown, the p-yH2AX stain suggests that it corresponds to a time point earlier than 2 w/o, regardless of this being the stage at which the first histological

difference across genotypes is observed. The presence of sertoli cell-only tubules during the 1st wave of spermatogenesis suggests a defect in the progenitor stem cell population (gonocytes), potentially in its replication capacity or migration efficiency across the gonads. The loss of stemness, however, is an unlikely explanation for this sertoli-cell only observation since *Ccna2*$^{myc-/myc-}$ testes are only delayed compared to the control groups during the 1st wave and there is still clear expression of the PLZF marker, which is involved in maintaining stem-like properties in cells (Costoya *et al*, 2004).

From a general point of view, the *Ccna2*$^{myc-}$ allele expression profile appears to be inverted when compared to the controls. Expression appears to be lower during the first two postnatal weeks, which are known to be highly proliferative instances for the SSC population. On the other hand, there appears to be an excessive expression of *Ccna2*$^{myc-}$ half way through the 1st wave of spermatogenesis, where the second wave begins and degeneration is observed, and in developed tissue, where stem cells should be be relatively quiescent. This type of transcriptional activity, upregulation in proliferative tissue and downregulation in quiescent, is a characteristic regulatory program for the E2F family of transcription factors, and its inversion in the mutants could be explained by the promoter mutation.

The high levels of expression of the *Ccna2*$^{myc+}$ allele at the 1 w/o time point temporally corresponds with the mitotic expansion of the spermatogonial population in wild-type mice (Kluin & Rooij, 1981), so the two-fold decrease in expression of the *Ccna2*$^{myc-}$ allele could cause a reduction in the number of total SSCs, the number of cycling SSCs, or both, in the promoter mutants. Although no IHC/IF stains were done on 1 w/o tissue due to the lack of sufficient biological samples across genotypes for statistical analysis at this time point, inferences can be extrapolated from the analyses done on the 2 w/o time point. The data generated with algorithm 2 (Mitotic activity analysis of SSCs) shows a decrease in total and cycling PLZF^{+} cells at 2 w/o; due to the delayed nature of the 1st wave of spermatogenesis in the promoter mutants, it is very likely that the tubules have a similar delayed trend between genotypes at 1 w/o. Further quantitative studies of

specific stem cell populations must be performed via marker analysis if the consequences of low levels of *Ccna2*$^{myc-}$ expression relative to the control at 1 w/o are to be elucidated.

Ccna2 expression follows a down-regulatory trend in both groups at 2 w/o, when the first sign of atrophy in the mutant is observed through histological analysis. At this time point, most *Ccna2*$^{myc+/myc+}$ tubules have reached the Zygotene stage of spermatid differentiation, while *Ccna2*$^{myc-/myc-}$ tubules appear to be delayed at the Preleptotene/Leptotene stage, where DSBs are induced (Ahmed *et al.,* 2013). This agrees with the p-yH2AX stain, where there are almost no tubules positive for DNA damage. The total SSC population as well as the fraction of cycling SSCs also appears to be low, in accordance with the quantitative analysis. Interestingly, a small fraction of *Ccna2*$^{myc-/myc-}$ tubules appears to be able to progress to the zygotene stage at 3 w/o regardless of their advancing degeneration and subsequently to the pachytene stage at 4 w/o. Apart from the fact that these surviving tubules were still delayed in the progression of the 1st wave of spermatogenesis relative to the control lines, this variability across the seminiferous tubules of *Ccna2*$^{myc-/myc-}$ mice contrasts greatly against the synchronous differentiation of the control lines.

The sudden upregulation of *Ccna2*$^{myc-}$ allelic expression during the following 3 and 4 w/o time points, where severe degeneration is observed, also coincides with the upregulation of SSCs and its proliferative activity. The following two time points, 6 and 12 w/o, also maintain higher levels of *Ccna2*$^{myc-}$ expression relative to the control, and display an active and expanded stem cell population. The SSC population has been reported to expand and differentiate in response to signals from Sertoli Cells that detect the loss of spermatogenic populations in the tubule (Rojas *et al.*, 2017). This would explain the sudden and prolonged upregulation of *Ccna2* expression seen in promoter mutants, since it coincides with the severe degeneration at 3 and 4 weeks, but also with the failed spermatogenic cycles of later time points.

This lack of fertility in adults, even with partial recuperation of cell populations, and the over activity of the SSC population suggests that the spermatogenic cycle is still

compromised and that viable sperm production is hindered. However, this failure to produce viable sperm in adulthood is blatantly different from the 1st wave's severe loss of differentiating populations. This distinction could be explained by the different identities of the progenitor cells responsible for the production of diff-SSCs for spermatogenesis in the 1st wave and then the subsequent ones. As previously discussed, gonocytes divide asymmetrically during the 1st wave, directly producing the diff-SCCs that feed into spermatogenesis. For the subsequent waves, the SSCs (that also arose from gonocytes) are the ones responsible for the maintenance of diff-SSCs. If the gonocyte-to-diff-SSC transition has different transcriptional regulatory needs compared to the SSC-to-diff-SSC transition, then *Ccna2* misregulation in both of these could account for the observed differences between the 1st and subsequent waves.

In terms of the gonocytes, it is possible that they require a quick upregulation of *Ccna2* expression for this transition as well as for the proper establishment of the SSC population, requiring E2F activators such as E2F1 that are unable to bind in the $Ccna2^{myc-}$ allele due to the promoter mutation. The lack of $Ccna2^{myc-}$ upregulation in these stages could prevent the CCNA2/CDK2 complex from performing its known functions such as aiding in DNA synthesis and induction of DSBs for recombination. Therefore, the lack of *Ccna2* upregulation during 1 and 2 w/o (after this asymmetric division of gonocytes) might halt SSC expansion as well as delay spermatogenesis until CCNA2 levels accumulate in these cells to induce DSBs for recombination, which is why there is a histological delay at the 2 w/o and decreased levels of $PLZF^{+}$ cells.

Once these tubules begin to degenerate going into the meiotic stages of the 1st wave, it is possible that sertoli cells signal the SSC population to expand and repopulate the mutant tubules, which is why there are higher counts of MYC^{++}, $PLZF^{+}$, and $PLZF^{+}/MYC^{++}$ cells in the analyzed images. However, this upregulation of $Ccna2^{myc-}$ transcription, potentially for the expansion and differentiation of the SSC population, does not rescue fertility. SSC progenitors might not be able to repress the induced overexpression of $Ccna2^{myc-}$ during later stages of meiosis due to the lack of E2F repressors such as E2F8 binding in the mutated E2F site. Such lack of repression might cause CCNA2/CDK2 to over-

induce DSBs as well as prevent the CCNA1/CDK2 complex from forming and repairing these unresolved DSBs. This hypothesis is also supported by the p-yH2AX stains in adult *Ccna2*$^{myc/myc-}$ tubules, where there appears to be a strong presence of spermatocytes with high p-yH2AX stain, which most likely corresponds to unresolved DSBs. Therefore, the combined effect of the lack of *Ccna2* expression downregulation in spermatocytes and the expansion of SSCs meant to compensate for the loss of testicular cell populations could account for the sustained upregulation of *Ccna2* after the 1st spermatogenic wave. One potential experiment that would test this hypothesis would be to isolate diff-SSCs (NGN3^{-}/KIT^{+}) from both the 1st and subsequent waves of spermatogenesis from all mouse lines via Fluorescence-Activated Cell Sorting (FACS) and analyze their relative CCNA2 levels. If the *Ccna2*$^{myc-/myc-}$ diff-SSCs contain significantly lower levels of CCNA2 during the 1st wave relative to the controls, and then significantly higher levels post-1st wave, then this hypothesis would become even more plausible.

As a whole, these observations suggest that transcriptional misregulation of *Ccna2* has multiple consequences in various spermatogenic populations, ultimately causing infertility. When it is not upregulated properly during early stages of the 1st wave of spermatogenesis and possibly during gonadal development, this initial wave is unsuccessful and experiences an almost complete loss of meiotic populations as well as lower total SSC and cycling SSC counts. However, when *Ccna2* is overexpressed in what seems to be a response to the severe degeneration, production of viable sperm is also hindered, potentially due to unresolved DSBs caused by lack of *Ccna2*$^{myc-}$ downregulation in spermatocytes. Taken together, the data suggests that the temporal specificity of *Ccna2* expression required for optimal CDK activity during spermatogenesis depends on both E2F activators and repressors, explaining the malfunctioning of the spermatogenic cycle when *Ccna2*'s canonical E2F binding site is mutated.

VII. **Conclusion**

The profound and dynamic effects the loss of E2F regulation on *Ccna2* causes in spermatogenesis illustrate the intricate system that is the cell cycle and its regulation. *In vivo* knock-in models such as the one used in this study allow for the participation of E2F regulation in physiological processes to manifest itself, and targeted mutation of single binding sites from specific targets are likely to continue revealing novel phenotypes. These findings further demonstrate the local and temporal specificity of expression E2F regulation can produce, allowing multiple targets to participate in complex processes at different tissues, like the testes. Since many of their targets are known to be upregulated in multiple cancers and typically perform conserved roles throughout evolution, their individual regulation by E2Fs should be of major interest and of continuous study.

VIII. **References**

Ahmed, E. A., Sfeir, A., Takai, H., & Scherthan, H. (2013). Ku70 and non-homologous end joining protect testicular cells from DNA damage. *Journal of Cell Science, 126*(14), 3095-3104. doi:10.1242/jcs.122788

Asian Journal of Andrology. (n.d.). Important Stages of Spermatogenesis. Retrieved August 07, 2017, from http://www.ajandrology.com/viewimage.asp?img=AsianJAndrol_2015_17_4_529_151397_f1.jpg

Blanco-Rodríguez, J. (2009). γH2AX marks the main events of the spermatogenic process. *Microscopy Research and Technique, 72*(11), 823-832. doi:10.1002/jemt.20730

Costoya, J. A., Hobbs, R. M., Barna, M., Cattoretti, G., Manova, K., Sukhwani, M., . . . Pandolfi, P. P. (2004). Essential role of Plzf in maintenance of spermatogonial stem cells. *Nature Genetics, 36*(6), 653-659. doi:10.1038/ng1367

Diril, M. K., Ratnacaram, C. K., Padmakumar, V. C., Du, T., Wasser, M., Coppola, V., . . . Kaldis, P. (2012). Cyclin-dependent kinase 1 (Cdk1) is essential for cell division and suppression of DNA re-replication but not for liver regeneration. *Proceedings of the National Academy of Sciences, 109*(10), 3826-3831. doi:10.1073/pnas.1115201109

Enserink, J. M., & Kolodner, R. D. (2010). An overview of Cdk1-controlled targets and processes. *Cell Division, 5*(1), 11. doi:10.1186/1747-1028-5-11

Gao, T., Han, Y., Yu, L., Ao, S., Li, Z., & Ji, J. (2014). CCNA2 Is a Prognostic Biomarker for ER Breast Cancer and Tamoxifen Resistance. *PLoS ONE, 9*(3). doi:10.1371/journal.pone.0091771

Hermo, L., Pelletier, R., Cyr, D. G., & Smith, C. E. (2009). Surfing the wave, cycle, life history, and genes/proteins expressed by testicular germ cells. Part 1: Background to spermatogenesis, spermatogonia, and spermatocytes. *Microscopy Research and Technique, 73*(4), 241-278. doi:10.1002/jemt.20783

Kluin, P. M., & Rooij, D. G. (1981). A comparison between the morphology and cell kinetics of gonocytes and adult type undifferentiated spermatogonia in the mouse. *International Journal of Andrology, 4*(1-6), 475-493. doi:10.1111/j.1365-2605.1981.tb00732.x

Lipshultz, L. I., Howards, S. S., & Niedeberger, C. S. (2009). *Infertility in the male*. Cambridge: Cambridge University Press.

Mahadevaiah, S. K., Turner, J. M., Baudat, F., Rogakou, E. P., Boer, P. D., Blanco-Rodríguez, J., . . . Burgoyne, P. S. (2001). *Nature Genetics, 27*(3), 271-276. doi:10.1038/85830

Manku, G., & Culty, M. (2015). Mammalian gonocyte and spermatogonia differentiation: recent advances and remaining challenges. *Reproduction, 149*(3). doi:10.1530/rep-14-0431

Morgan, D. A. (2007). The Cell Cycle: Principles of Control. *Cell Division, 2*(1), 27. doi:10.1186/1747-1028-2-27

Ortega, S., Prieto, I., Odajima, J., Martín, A., Dubus, P., Sotillo, R., . . . Barbacid, M. (2003). Cyclin-dependent kinase 2 is essential for meiosis but not for mitotic cell division in mice. *Nature Genetics, 35*(1), 25-31. doi:10.1038/ng1232

Payne, C. J. (2013). Cycling to and from a stem cell niche: the temporal and spatial odyssey of mitotic male germ cells. *The International Journal of Developmental Biology, 57*(2-3-4), 169-177. doi:10.1387/ijdb.130006cp

Rebourcet, D., O'Shaughnessy, P. J., Monteiro, A., Milne, L., Cruickshanks, L., Jeffrey, N., . . . Smith, L. B. (2014). Sertoli Cells Maintain Leydig Cell Number and Peritubular Myoid Cell Activity in the Adult Mouse Testis. *PLoS ONE, 9*(8). doi:10.1371/journal.pone.0105687

Revolvy, L. (n.d.). "Cyclin A" on Revolvy.com. Retrieved August 07, 2017, from https://www.revolvy.com/topic/Cyclin%20A&uid=1575

Rojas, J., L., Fahiel, C., & Socorro, R. M. (2017). Stress and Cell Death in Testicular Cells. *Journal of Antimicrobial Agents, 06*(01). doi:10.4172/2167-0250.1000183

Rédei, G. P. (2008). G1 Phase. *Encyclopedia of Genetics, Genomics, Proteomics and Informatics*. doi:10.1007/978-1-4020-6754-9_6354

Satyanarayana, A., & Kaldis, P. (2009). Mammalian cell-cycle regulation: several Cdks, numerous cyclins and diverse compensatory mechanisms. *Oncogene, 28*(33), 2925-2939. doi:10.1038/onc.2009.170

Szostak, J. W., Orr-Weaver, T. L., Rothstein, R. J., & Stahl, F. W. (1983). The double-strand-break repair model for recombination. *Cell, 33*(1), 25-35. doi:10.1016/0092-8674(83)90331-8

Tane, S., & Chibazakura, T. (2009). Cyclin A overexpression induces chromosomal double-strand breaks in mammalian cells. *Cell Cycle, 8*(23), 3900-3903. doi:10.4161/cc.8.23.10071

Thurlings, I., & Bruin, A. D. (2016). E2F Transcription Factors Control the Roller Coaster Ride of Cell Cycle Gene Expression. *Methods in Molecular Biology Cell Cycle Oscillators,* 71-88. doi:10.1007/978-1-4939-2957-3_4

Viera, A., Alsheimer, M., Gomez, R., Berenguer, I., Ortega, S., Symonds, C. E., . . . Suja, J. A. (2014). CDK2 regulates nuclear envelope protein dynamics and telomere attachment in mouse meiotic prophase. *Journal of Cell Science, 128*(1), 88-99. doi:10.1242/jcs.154922

Wolgemuth, D. J., Lele, K. M., Jobanputra, V., & Salazar, G. (2008). Function of cyclins in regulating the mitotic and meiotic cell cycles in male germ cells. *Cell Cycle, 7*(22), 3509-3513. doi:10.4161/cc.7.22.6978

Wolgemuth, D. J. (2011). Function of the A-Type Cyclins During Gametogenesis and Early Embryogenesis. *Results and Problems in Cell Differentiation Cell Cycle in Development,* 391-413. doi:10.1007/978-3-642-19065-0_17

Wolgemuth, D. J., Manterola, M., & Vasileva, A. (2013). Role of cyclins in controlling progression of mammalian spermatogenesis. *The International Journal of Developmental Biology, 57*(2-3-4), 159-168. doi:10.1387/ijdb.130047av

Yang, Rong, et al. "Functions of Cyclin A1 in the Cell Cycle and Its Interactions with Transcription Factor E2F-1 and the Rb Family of Proteins." *Molecular and Cellular Biology*, vol. 19, no. 3, Jan. 1999, pp. 2400–2407., doi:10.1128/mcb.19.3.2400.

Yoshida, S., Takakura, A., Ohbo, K., Abe, K., Wakabayashi, J., Yamamoto, M., . . . Nabeshima, Y. (2004). Neurogenin3 delineates the earliest stages of spermatogenesis in the mouse testis. *Developmental Biology, 269*(2), 447-458. doi:10.1016/j.ydbio.2004.01.036

IX. **Supplemental Figures**

Table 1: ID and dilutions of antibodies used for IHC/IF stains.

Antibody ID	Antibody dilution
myc-Tag (CST 2278)	1:100
PLZF (Santa Cruz sc-22839)	1:200
p-γH2AX S139 (CST 9718)	1:300

Table 2: InForm algorithms designed for IHC/IF quantification stains

Stain	Description of Algorithms used for quantification
PLZF/ MYC	**Algorithm 1 – Analysis of cell population with high levels of CCNA2.** ➢ A low threshold for DAPI nuclear positivity was used to quantify all of the cells per image. ➢ Then, a signal intensity threshold of 0.225 on a scale of 0-1 (where the cell with the lowest MYC fluorescence signal detected in the image corresponds to 0) was used to quantify the fraction of cells positive for this established threshold (MYC^{++}) ➢ By multiplying the fraction of cells positive for the established threshold with the total number of cells, the total number of MYC^{++} cells per picture was quantified.
	Algorithm 2 - Mitotic activity analysis of SSCs ➢ A low intensity threshold for PLZF-positivity was used to quantify the total number of SSCs ($PLZF^{+}$) per image. ➢ Then, using a high intensity threshold for MYC-positivity of 0.7 on a scale of 0-1 (where the cell with the lowest MYC fluorescence signal detected in the image corresponds to 0) the fraction of $PLZF^{+}$ cells with high levels of CCNA2 ($PLZF^{+}/MYC^{++}$) was quantified. ➢ By multiplying this fraction by the total number of $PLZF^{+}$ cells per picture, the total number of $PLZF^{+}/MYC^{++}$ cells per picture was also quantified.
p-yH2AX	**Algorithm 3 – DSB induction and repair assessment (CCNA2/CDK2 Function).** ➢ Using standard counter-stain nuclear segmentation, the total number of cells per image was quantified. ➢ Then, using a 0.7 intensity threshold for p-yH2AX-positivity, on a scale of 0 to 1, where the cell with the lowest DAB signal detected in the image corresponds to 0, the fraction of cells with high DNA damage/DSBs ($p\text{-}yH2AX^{++}$) was quantified. ➢ By multiplying this fraction by the total number of cells per picture, the total number of $p\text{-}yH2AX^{++}$ cells per picture was quantified.

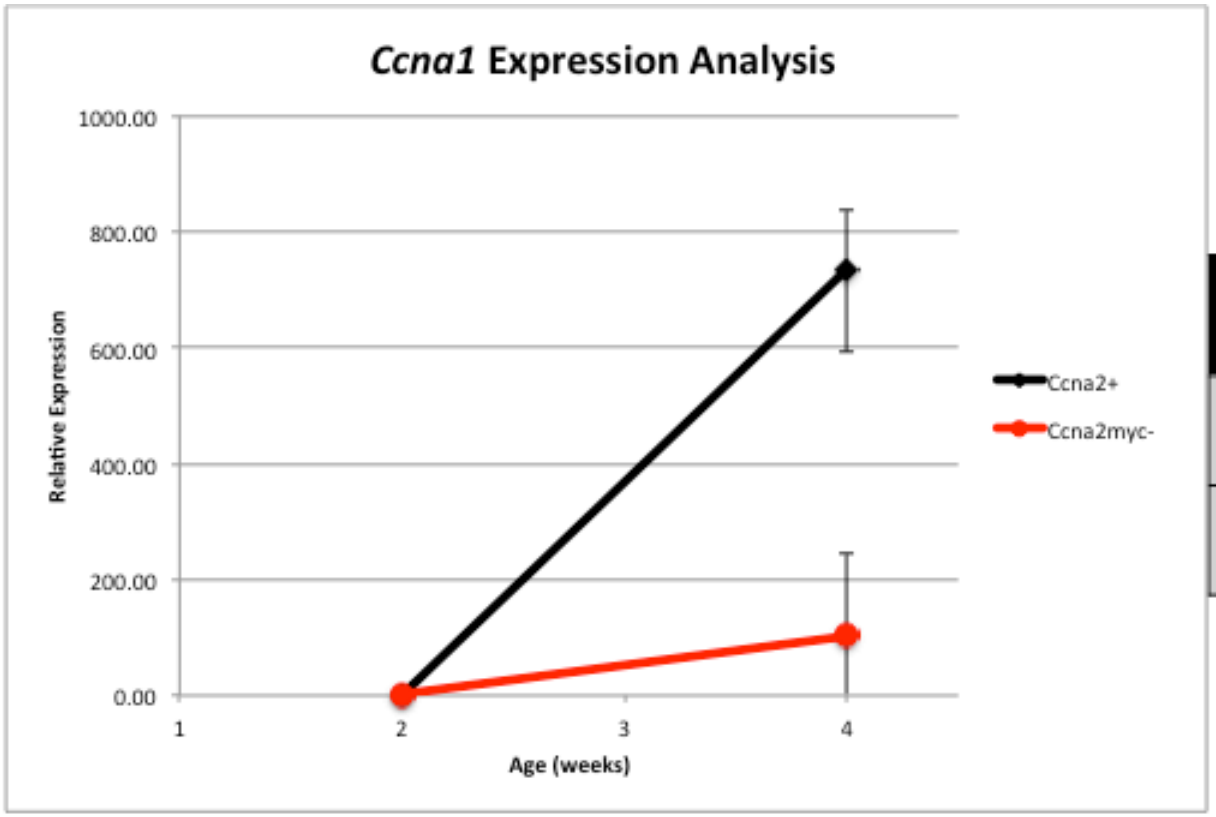

Time point	Genotype	Avg Relative expression
2 w/o	Ccna2+	1.0 (n=2)
	$Ccna2^{myc-}$	2.3 (n=2)
4 w/o	Ccna2+	735.2 (n=2)
	$Ccna2^{myc-}$	102.3 (n=4)

Supplemental Figure 1: Relative *Cyclin A1* expression analysis during the 1st wave of spermatogenesis via qPCR. *Ccna1* transcription was analyzed across the 2 and 4 w/o time points. The data shows a lack of *Ccna1* transcription in both lines at 2 w/o relative to the later time point. This is expected since the meiotic populations that express *Ccna1* are not supposed to be present at such an early time point. However, there is a pronounced lack of *Ccna1* transcription in promoter mutants at 4 w/o relative to the wild type, which is when the seminiferous tubules are predominantly populated by meiotic cell populations, many of which express the meiosis-specific *Ccna1*. Statistical analyses were not performed due to the low number of biological replicates.